



Bioheat Modelling and Simulation for Body Heat Powered Medical Implants

By:

Ujjwal Verma

Fakultät für Informatik und Elektrotechnik

University of Rostock

A thesis submitted in the partial fulfilment of
M.Sc. in Computation Science and Engineering

July 2018

Under the guidance of:

Prof. Dr.-Ing. Dennis Hohlfeld

Dipl.-Ing. Stefanie Kreß

Abstract

Implantable medical devices, more specific electrically active implants, have found success in clinical trials. These are gaining interest especially for treatments like bone tissue regeneration and treating motion disorders using deep brain stimulation. These new generation of implants require continuous and sufficient electrical power to ensure optimal operation. Currently the implants are powered using non-rechargeable batteries, which once depleted are a major reason for re-intervention surgeries. Harvesting the available ambient thermal energy from the human body provides a likely solution to improve the implant's lifetime. The human body being subjected to laws of thermodynamics maintains a body core temperature of 37 °C with the skin surface being the heat exchanging medium with the environment and the fat layer acting as a thermal insulator. This leads to a natural thermal gradient inside the body. Subcutaneous thermoelectric energy harvesting using this thermal gradient inside the human body can be utilized for powering these implants.

In the scope of this thesis, simulations of the human thermal system are performed. Various aspects of heat transfer such as metabolic heat generation, blood perfusion along with sensible and insensible heat loss mechanisms are implemented. Open source finite element modelling compatible geometry of the human body generated with data from magnetic resonance imaging and computer tomography is used. Finally a simple thermoregulatory system is presented with vasoconstriction, vasodilation and sweating. The outcome of this work is the temperature distribution inside a realistic human body model that can be of future use for identification of potential implant locations.

Keywords: *Bioheat, Human body heat transfer, Thermoregulation*

Declaration

I hereby declare that I, Ujjwal Verma, have written this document independently and all the sources of information and aid have been acknowledged to the best of my knowledge. This document has not been submitted previously for any other qualification at any other universities or institutions. This thesis is based on work done by myself under the guidance of my supervisors.

.....

.....

Location, Date

Signature

Acknowledgements

I would like to express my deep gratitude to Prof. Dr.-Ing. Dennis Hohlfeld for providing me with the opportunity to work on this topic and spending his precious time to guide me during this master thesis. Without his continuous supervision and valuable inputs, this work would not have been possible.

Furthermore, I would like to thank Dipl.-Ing. Stefanie Kreß for her support and suggestions on various aspects throughout this thesis. I am also grateful for her patience and constructive comments during the compilation of this text.

Finally, I would also like to thank my parents and my sisters for their unconditional love, support and encouragement throughout this journey, this accomplishment would not have been possible without them.

Contents

List of figures.....	iii
List of tables.....	v
List of Notations	vi
1 Introduction	1
1.1 Motivation	2
1.2 Overview.....	4
2 Literature review.....	5
3 Theoretical background	9
3.1 The passive human thermal system.....	9
3.1.1 Internal heat transfer	9
3.1.2 External heat transfer.....	12
3.2 The active human thermal system	16
3.2.1 Shivering	18
3.2.2 Vasomotor response	18
3.2.3 Sweating	20
3.3 Thermoelectric generators	20
4 Simulation methodology.....	23
4.1 Stationary heat transfer in humans.....	23
4.1.1 Simplified cubic human tissue.....	31
4.1.2 Simplified human forearm.....	33

4.1.3	Human forearm	34
4.1.4	Torso	36
4.2	Thermoregulatory control loop (Transient analysis).....	37
5	Results and discussion	41
5.1	Stationary heat transfer in humans.....	41
5.1.1	Simplified cubic human tissue.....	41
5.1.2	Simplified human forearm.....	42
5.1.3	Human forearm	43
5.1.4	Torso	47
5.2	Thermoregulation in simplified cubic model	50
6	Conclusion and Outlook.....	53
7	References	55
8	Appendix.....	I
8.1	APDL commands.....	I
8.2	Analysis settings	VIII
8.3	Torso model details	VIII
8.4	Supplementary results.....	IX

List of figures

Figure 1: Embedded TEG in human body tissue.....	3
Figure 2: (a) Wissler's model with 15 nodes [17], (b) Fiala's passive model with 15 nodes divided further into three subsectors [20]	8
Figure 3: Heat loss mechanisms (a) Radiation, (b) Convection, (c) Evaporation [26]	12
Figure 4: Variation in heat transfer mechanisms with temperature [29].....	17
Figure 5: Representation of the active system of the Stolwijk's 25-node model [15].....	17
Figure 6: (a) Capillary bed showing the branching of blood vessels [30], (b) Change of blood vessel diameter in case of vasoconstriction and vasodilation [26].....	19
Figure 7: TEG with ceramic plates, thermocouples and copper interconnects	21
Figure 8: Process flow of simulation setup.....	26
Figure 9: Table definition for temperature dependent heat generation based on Table 528	
Figure 10: Table definition for temperature dependent evaporative heat flux	30
Figure 11: VHP-Female V.2.2 human model displayed in MATLAB environment [38]	31
Figure 12: (a) The simplified human tissue model with muscle, subcutaneous fat and skin; (b) Dimensions of the model	32
Figure 13: Hexahedral meshed model with boundary conditions	33
Figure 14: Simplified human forearm with muscle fat and skin along with blood vessels and bone.....	34
Figure 15: Human forearm model with internal bones and blood vessels	35
Figure 16: Boundary conditions for the human forearm at 15 °C.....	35
Figure 17: Human torso model with different tissue structures.....	36
Figure 18: Boundary conditions for the human torso at 15 °C	37
Figure 19: Control loop for current implantation of thermoregulation.....	39
Figure 20: Temperature distribution along central axis of simplified cubic human tissue.	41
Figure 21: Contour plot of temperature distribution on simplified human forearm	42
Figure 22: Temperature distribution along the path close to blood vessel in simplified human forearm.....	43
Figure 23: Contour plot of temperature distribution on realistic human forearm.....	44
Figure 24: Path inside the human forearm	44

Figure 25: Temperature profile along path (Figure 24) in realistic human forearm at 15 °C	45
Figure 26: Comparison of ANSYS results with Pennes' measurements at 26.6 °C	46
Figure 27: Temperature along long axis of arm at 25 °C compared to Pennes' measurements	46
Figure 28: Various temperatures of the forearm in different environmental conditions ..	47
Figure 29: Torso, front view	48
Figure 30: Torso, front view - section.....	48
Figure 31: Torso, side view	48
Figure 32: Torso, side view - section	48
Figure 33: Torso, cross-sectional distribution	49
Figure 34: Torso, internal distribution.....	49
Figure 35: Temperature profiles along 3 sections from Figure 33.....	50
Figure 36: Temperature distribution of initial state and after control at 15 °C.....	51
Figure 37: Temperature distribution of initial state and after control at 25 °C.....	51
Figure 38: Analysis settings for stationary simulations.....	VIII
Figure 39: Temperature contour of simplified cubic geometry at 15 °C	IX
Figure 40: Temperature along central path in simplified human forearm	IX
Figure 41: Muscle and skin temperature over time at 15 °C	X
Figure 42: Muscle and skin temperature over time at 25 °C	X

List of tables

Table 1: Power requirements of medical devices [4].....	2
Table 2: Contribution of various heat transfer mechanisms towards heat loss [27].....	13
Table 3: Average thermal properties of tissues from the IT'IS database [34]	24
Table 4: Averaged and minimum value for metabolic heat generation and perfusion rate [34].....	25
Table 5: APDL command for the bioheat implementation as heat generation load	28
Table 6: APDL command for evaporative heat loss as heat flux.....	30
Table 7: Components of the three controllers based on control scheme	39
Table 8: APDL command for evaporative heat loss	I
Table 9: APDL command for heat generation for tissue	III
Table 10: APDL command for control in active system.....	III
Table 11: Heat generation load application for torso	VII
Table 12: Adjusted metabolic heat generation rates for torso model	VIII

List of Notations

Symbol	Description	Units
A	Area	m^2
A_{skin}	Area of skin surface	m^2
Bf	Blood flow signal	-
c	Specific heat capacity of tissue	$\text{J}/(\text{kg K})$
c_b	Specific heat capacity of blood	$\text{J}/(\text{kg K})$
C_{res}	Dry respiration heat loss per unit body surface area	W/m^2
C_s	Cutaneous vasoconstriction	-
$C_{\text{SIG}_{\text{sk}}}$	Effector-controlling signal for vasoconstriction (skin)	-
$C_{\text{SIG}_{\text{cr}}}$	Effector-controlling signal for vasoconstriction (core)	-
Dl	Cutaneous vasodilatation	-
$e(t)$	Error between controlled variable	-
E_{res}	Evaporative loss from respiration	W/m^2
\dot{E}_{skin}	Total evaporative heat loss from the skin	W/m^2
F	View factor	-
h_c	Convective heat transfer coefficient	$\text{W}/(\text{m}^2 \text{ K})$
h_e	Evaporative heat transfer coefficient	$\text{W}/(\text{m}^2 \text{ kPa})$
K_p	Proportional gain	-
M	Metabolic free energy production per unit body area	W/m^2
M_{shiv}	Component of metabolic heat due to shivering	W/m^2
M_w	Component of metabolic rate due to type of work	W/m^2
n	Number of thermocouple	-
P_a	Partial pressure of water vapour in air	kPa
P_{sa}	Saturated vapour pressure	kPa
P_{out}	Output signal from controller	-
P_{max}	Maximum power output	W
$P_{\text{sk},s}$	Saturated water vapour pressure at skin temperature	kPa

q_{cond}	Heat transfer by conduction	W/m ²
q_{conv}	Convective heat loss per unit area	W/m ²
q_{rad}	Radiative heat loss per unit area	W/m ²
q_{sk}	Total heat loss at the skin	W/m ²
Q_m	Metabolic rate	W/m ³
$Q_{m,bas,0}$	Basal metabolic rate at thermal neutrality	W/m ³
$Q_{m,sh}$	Metabolic rate due to shivering	W/m ³
$Q_{m,w}$	Metabolic rate due to external work	W/m ³
R_{el}	Electrical resistance	Ω
T	Tissue temperature	K
T_0	Tissue temperature at thermal neutrality	K
T_{artery}	Artery temperature	K
T_{skin}	Skin temperature	K
T_{amb}	Ambient temperature	K
$T_{sk,m}$	Mean skin temperature	K
T_{hy}	Hypothalamus temperature	K
$T_{sk,0}$	Skin temperature at thermal neutrality	K
\bar{T}	Average temperature between the hot and cold surfaces	K
ΔT	Temperature difference across peltier leg	K
v	Wind velocity	m/s
w	Skin wettedness	-
ω_{sk}	Perfusion rate in skin	1/s
$\omega_{sk,0}$	Perfusion rate in skin at thermal neutrality	1/s
ω_b	Perfusion rate in tissue	1/s
V_{out}	Output voltage	V
ZT	Figure of merit	-

Greek

α	Distribution coefficient	-
α_n	Seebeck coefficient of n-type semi-conductor	V/K
α_p	Seebeck coefficient of p-type semi-conductor	V/K
ε	Emissivity	-
κ	Thermal conductivity of tissue	W/(m K)
κ_n	Thermal conductivity of n-type semi-conductor	W/(m K)
κ_p	Thermal conductivity of p-type semi-conductor	W/(m K)
ρ	Density of tissue	kg/m ³
ρ_b	Density of blood	kg/m ³
ρ_n	Resistivity of n-type semi-conductor	Ω m
ρ_p	Resistivity of p-type semi-conductor	Ω m
σ	Stefan–Boltzmann constant = 5.67×10^{-8}	W/(m ² K ⁴)
σ_n	Electrical conductivity of n-type semi-conductor	S/m
σ_p	Electrical conductivity of p-type semi-conductor	S/m
ϕ	Relative humidity	-

Abbreviations

APDL	ANSYS parametric design language
ARG	Argument
BFE	Body force element
CFD	Computational fluid dynamics
CT	Computed tomography
HGEN	Heat generation
IMD	Implantable medical devices
MRI	Magnetic resonance imaging
PID	Proportional-integral-derivative controller
TEG	Thermoelectric generator

1 Introduction

The modern industrialized world has facilitated increased life expectancy of the aging population, this has led to a subsequent growth in field of biomedical innovation. A large number of implantable medical devices (IMD) are available today as a product of cooperative efforts between engineers and medical professionals. Continued demands are only going to further advance current medical devices, extending their scope beyond today's clinical environment and into household healthcare systems. A glimpse into the future of these devices is evident in the current generation of smart implants, one such example is that of advanced pacemakers with wireless communication for patient monitoring [1].

All these implants require electrical energy to fulfill their function. Battery technology has come a long way since 1958 when the first pacemaker implantation used nickel-cadmium batteries, currently lithium batteries are used as a standard source of power. Increased functionality comes at the cost of greater power expenditure, this has exposed the disparity in current lithium chemistry as a sustainable option for future implants. According to a study, individuals with pacemakers powered by lithium batteries require a reoperation every 7 or 8 years; most commonly for replacement of the battery [2]. This in turn adds unnecessary risks and costs for the patient. Without any significant progress in energy storage technology, the lifetime of the implantable device is rather limited.

Many alternative methods have been explored for substituting the lithium batteries, e.g. bio-fuel cells that use glucose as a fuel to power the implant, and nuclear cells for pacemakers, but due to an added risk of radiation poisoning and reliability concerns this is not a viable option [3]. While these methods are an improvement towards energy autonomy, they still have certain drawbacks such as high cost, possible contamination or inadequate performance, etc. To ensure proper operation, implants need to rely on continuous and sufficient power supply. Through rapid development in engineering and increased efficiency, today's implants have reduced energy requirements, but a reliable and perpetual source of power has not yet been established. From Table 1 the typical energy expenditure for various implantable devices are available, ranging from 30 μW to several mW [4].

Table 1: Power requirements of medical devices [4]

Implantable medical device	Typical power requirement
<i>Pacemaker</i>	30 ~ 100 μ W
<i>Cardiac defibrillator</i>	30 ~ 100 μ W
<i>Neurological stimulator</i>	30 μ W to several mW
<i>Drug pump</i>	100 μ W to 2 mW
<i>Cochlear implants</i>	10 mW

Given the low power requirements, the human body presents various opportunities for energy harvesting. These sources are in the form of kinetic energy from movement of joints, biomechanical vibrations and thermal energy. The body provides plentiful energy in the form of heat, the food consumed is used to maintain the body core temperature [3]. The natural abundance of thermal energy prompts for harvesting these sources by means of solid-state thermoelectric generators (TEG). This possible scavenging of waste heat offers a potential solution towards the increase in power demands of IMDs.

1.1 Motivation

The human body is a complex and fascinating system. The body consist of the central core and the peripheral shell. The core represents the thermoregulated deep tissues of inner organs, whereas the peripheral shell comprises of skin and the subcutaneous tissue. The skin acts as the heat exchanger with the environment. The manner in which the human body is able to maintain its core temperature at 37 °C through different thermoregulatory processes is a feat in itself. The body's response to various environmental changes plays a vital role for human survival. If the body does not loose heat to the environment, body temperature can rise by up to 1 °C every hour till the person's death [5].

A living person at rest generates about 100 W of energy through thermogenesis, low grade heat loss from the body accounts for about 80 % of this metabolic heat as a product of thermoregulation. This heat loss occurs at the skin surface in the form of sensible and insensible heat transfer such as radiation, convection and evaporation. Additionally, a small

amount of this heat is also lost due to respiration. As a direct consequence of heat loss, the skin surface is generally at a lower temperature than the body core with the fat layer acting as an insulator. Typically about 1–5 K temperature difference between the skin and the core can be observed in the certain regions of the body [6]. To find an optimal power output for operation inside the human body, *in silico* simulations of temperature distribution in human body are necessary to identify locations with highest temperature gradients. Figure 1 shows a TEG embedded inside the fat layer of a simplified human tissue.

The purpose of present study is to develop a thermal model of the human body that can be used to evaluate the temperature distribution inside the human body. Since the power output is dependent on the temperature difference across the TEG, careful identification of potential locations for TEG powered implant is of crucial importance. At first, stationary study on simplified models of tissue geometry is performed to test the heat generation in the tissue and the effect of various heat transfer mechanisms. Later, simulations are performed on realistic human body geometry such as the human forearm and the torso with appropriate material properties. Finally, a thermoregulation loop is developed to be applied on the simplified geometry with proportional control under transient condition. Controlled properties include metabolic heat generation, blood perfusion rate and heat loss due to evaporation on skin.

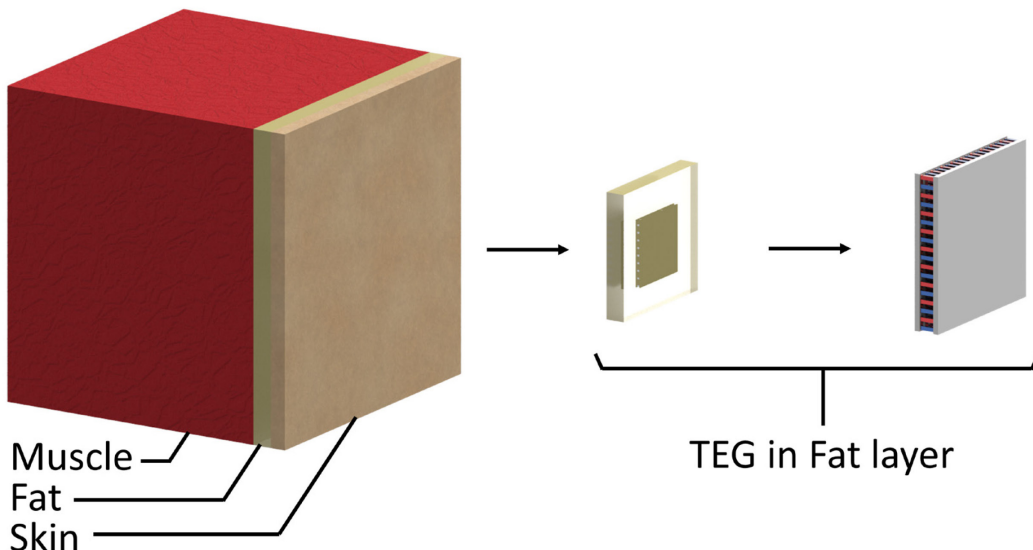


Figure 1: Embedded TEG in human body tissue

1.2 Overview

Chapter 1 provides an introduction to the energy problem of electrically active implants and the motivation that led to the work developed in this thesis.

In Chapter 2, a brief literature review for various state of the art thermal models for simulating the human body is discussed, while Chapter 3 highlights the fundamental theory related to both passive and active human thermal systems. This includes different types of heat loss mechanisms in the body.

Chapter 4 details the methodology utilized for the thermal simulations. Distributed among the subsections are the steps taken to perform the stationary analysis on various geometric models with different level of complexity, along with transient simulation of a basic thermoregulation control loop using the commercial simulation tool ANSYS Mechanical.

In Chapter 5, the results obtained and associated discussion are presented for different simulations. Finally, in Chapter 6 conclusions are drawn from the results and possible scope for future research is discussed. The Appendix provides some supplementary information such as APDL scripts and other additional results.

2 Literature review

In recent years thanks to increased access to more advanced computing power, computational modelling has proven to be a valuable addition to the research community. This has assisted continued contributions towards better understanding of the human body as well as development of advanced biomedical technologies. Modelling of more complex systems coupled with improved numerical methods has facilitated detailed analysis of the information collected, and further study the influence of several parameters.

The human body is highly receptive of any external stimuli; in day to day scenario, changes in environmental conditions necessitate the body to adapt so as to remain in a comfortable state. When drastic changes take place, the thermoregulatory system manages the amount of heat absorbed or released to maintain the core temperature. Numerical models are the backbone of any computational analysis. Although, it is reasonable to assume that any numerical model cannot be perfect; it is essential that the models capture the complexity of such a system up to an acceptable degree. Over the years many human thermal models have been presented. A brief overview of a few existing models is given below.

The heat transfer in biological tissue is one of the fundamental requirements of a model, the most significant contribution was that of Pennes in 1948 [7]. Energy balance equation utilizing basic thermodynamic laws was used for calculating heat transfer in the human forearm. The bioheat equation included the effects of metabolic heat generation and blood perfusion accounting for the effect of body core temperature and blood flow rate. The equation was presented as:

$$\rho c \frac{\partial T}{\partial t} = \nabla \kappa \nabla T + \rho_b c_b \omega_b (T_{artery} - T) + Q_m \quad (1)$$

where, ρ , c , T and κ are the density, specific heat, temperature and thermal conductivity of the tissue. T_{artery} is the arterial blood temperature, Q_m is the metabolic heat generation and ρ_b , c_b and ω_b are, respectively, the density, specific heat and perfusion rate of blood.

Certain assumptions such as neglecting blood flow direction, using body core temperature at the capillary beds and large blood vessels not affecting the heat transfer in capillaries have limited the usability to only basic applications. Due to this many two and three

equation based bio heat models have been proposed [8–10]; although these models account for various shortcomings of the Pennes' equation, detailed knowledge of vascular geometry is necessary. Despite its criticisms, the Pennes' bioheat equation has proven to be a valuable approximation for heat transfer within the tissue and is used extensively in various human thermal models and hypothermia based treatments. In 1998 Wissler revisited the original study, validated the results and proved the assumptions made by Pennes during the development of the model were reliable [11].

One of the first and most prominent 2-node model of human thermal system is that of Gagge et al. (1971) [12]. Two nodes comprised the core and the skin, where body core represented bone, muscle, internal organs, and subcutaneous tissue. Two energy balance equations were used to evaluate the thermal response for each node. The model involved various physical effects such as sensible heat transfer, convective transfer from blood flow, metabolic heat generation while exercising and shivering along with energy exchange with the surroundings. In 1986 the model was further improved by Gagge to include additional control capabilities with parameters such as sweat rate, blood flow rate, shivering metabolic rate [13]. A higher core temperature signal enabled vasodilation while a lower skin temperature led to vasoconstriction. A warmer signal from both nodes controlled the sweat rate for evaporative heat loss, while in colder temperatures the model varied rate of shivering thermogenesis. Given the model's simplicity its application was limited to only certain situations.

As a means to assess thermal responses of astronauts for NASA, Stolwijk (1971 and 1977) developed a 25-node model involving passive and active thermal system [14, 15]. The passive system incorporated various heat transfer mechanisms for internal and external heat transfer and the active system controlled various thermoregulatory aspects of the body such as vasomotor function, sweating and shivering. This model laid the foundation of many future thermal models. Unlike Gagge's model, Stolwijk divided the body into a sphere for the heat and individual cylinders for the hands, arms, trunk, legs and feet. Furthermore, concentric core, muscle, fat and skin layers were modelled on each of the six parts. The trunk also had the central blood pool as a separate node which was connected to every other tissue nodes by circulatory system of blood vessels. Conductive heat transfer was used between the tissue nodes, while the heat exchange between the tissue node

adjacent to the central blood node was via convection. Energy balance equations for each node included heat accumulation, blood convection, tissue conduction, metabolic generation, respiration and heat transfer to the environment by means of convection, radiation and evaporation. The control system had a temperature sensing sub-system with a simple thermoregulatory system operating in terms of controlling coefficients for the control values.

Gordon et al. (1976) presented a comprehensive regulatory system for the transient cold exposure response [16]. The model utilized individual thermophysical and material properties for tissues and expanded the Stolwijk model by providing nodes for the face, neck and forehead on the head. The trunk enclosed the thorax, abdomen and a separate lung region. The central pool of blood supplied blood to the major body sections, with the boundary condition at the skin modelled according to equation (2):

$$-A\kappa \frac{\partial T}{\partial r}\Big|_s = h_c A_{skin} (T_{skin} - T_{amb}) + \sigma \varepsilon F A_{skin} (T_{skin}^4 - T_{amb}^4) + \dot{E}_{skin} \quad (2)$$

Another important thermophysiological model was introduced by Wissler in 1964 and later updated in 1985 [17, 18]. The model featured highly detailed vascular network which comprised of arteries, veins and capillaries, with the temperature of blood assumed uniform. Initially the model consisted of 6 elements which was later increased to 15, which offered a considerably larger magnitude than the Stolwijk model. The vascular system originated from the heart in the trunk which spread out into arteries and then into capillaries for each element illustrated in Figure 2 (a). The blood then circulated back to the heart through the veins. Also modelled was the concurrent heat transfer between large arteries and veins with transient bioheat equation.

The Fiala model for the human thermal system was introduced with the passive system in 1998, 1999 and later extended to include the active system in 2001 [19–21]. 15 spherical and cylindrical nodes were each divided into anterior, posterior and inferior sectors with different parts: core, viscera, lung, muscle, fat, inner skin and outer skin (Figure 2 (b)). This extensive subdivision allowed customization of various tissue by providing appropriate tissue properties. For heat transfer in tissue Pennes' Bioheat equation (1) was used [7]. Perfusion acted as a heat exchange mechanism between the tissue and the blood. Heat exchange with the environment took place via convection, radiation, evaporation and

respiratory losses. For the active system, regression analysis was performed to determine the signal responses for individual thermoregulatory mechanisms. Vasodilation, vasoconstriction, shivering and sweating effects under various boundary conditions were assessed and validated.

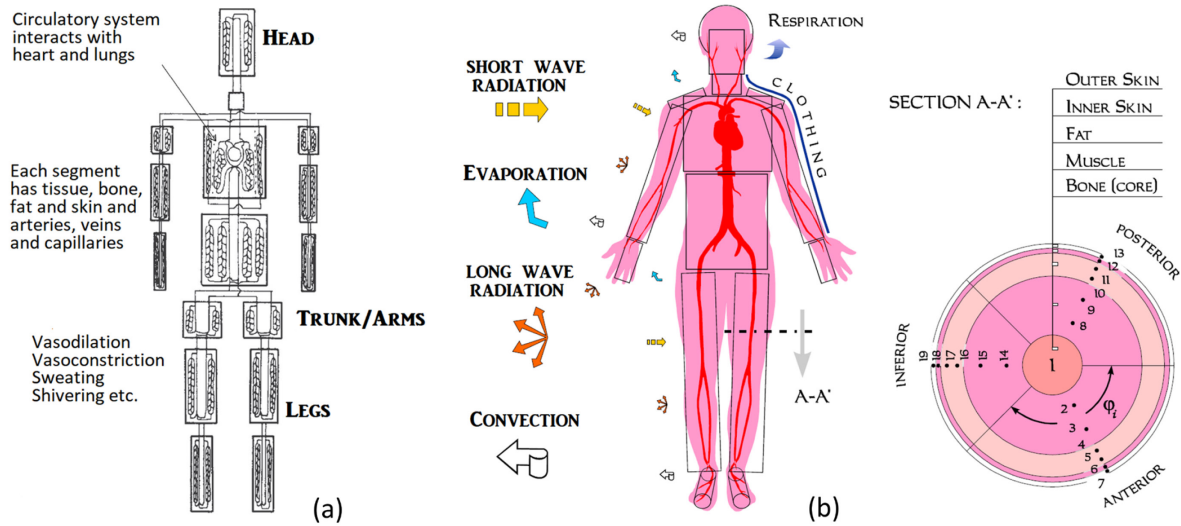


Figure 2: (a) Wissler's model with 15 nodes [17], (b) Fiala's passive model with 15 nodes divided further into three subsectors [20]

Other notable works include: the first 3D transient model developed by Smith which provided a highly realistic representation of the body along with a thermoregulatory system. The model also included a respiratory cycle to account for respiratory loss. The heat transfer equations were solved using finite element method for a simple mesh [22]. In 2007 Salloum et al. presented a highly sophisticated model consisting of 15 body segments. Each of the 15 segments was composed of four layers: the core, skin, artery blood and vein blood. Blood flow was simulated using actual physiological data relative to anatomic position of arteries [23].

As the human body is non-uniform across its sections, Werner et al. rather opted for a more fitting representation of the human body with individual organs as opposed to the more conventional symmetric geometries composed of cylinders [24]. Although the model was limited in its capabilities of physiological research, Werner concluded that studying the effects of the general inhomogeneity of the human body was important highlighting the use of temperature profiles within the body for its probable benefits for medical research.

3 Theoretical background

The general modelling of human thermal system is often divided into two systems. The passive system which incorporates the various heat transfer mechanisms inside the body along with skin surface phenomena and the active system which controls the thermoregulatory responses of factors such as blood flows by vasomotor reactions, shivering and sweating to maintain the body in an acceptable thermal condition.

3.1 The passive human thermal system

The passive thermal modelling is based on the general thermodynamic laws for heat transfer. Inside the body, metabolic heat is generated and this heat is then transported to body regions with the help of conduction and blood circulation. The subcutaneous fat layer acts as a thermal insulator for the body, the composition of fat is such that it only conducts about a third of the heat as compared to other tissues [25]. This maintains the body core at 37 °C by preventing unintended heat loss to the surroundings. Heat exchange with the environment takes place on the skin surface, heat is removed in the form of radiation, convection and evaporation. Additionally heat is lost via the respiratory track during the normal breathing cycle. Environmental factors such as ambient temperature, relative humidity, and wind speed play an important role in the amount of heat loss.

Based on the laws of thermodynamics for sensible and insensible heat loss, the heat-transfer processes are characterized into: Internal heat transfer and External heat transfer.

3.1.1 Internal heat transfer

To maintain the body core temperature, the body has to generate energy by processing the food ingested. Metabolism transforms the food into useable energy for the body and perfusion of blood allows transport of heat throughout the body. The three main contributions for internal heat transfer are: conduction, metabolic heat generation and blood perfusion.

Metabolic heat generation

Humans are endotherms, meaning they rely on internal body processes to generate heat and maintain a constant body temperature for survival. All the chemical reactions in every cell of the body contribute towards the metabolism process with heat being an essential product. Like most chemical reactions, a certain temperature is necessary to carry out these processes, for humans this temperature is about 37 °C. The energy is generated from breaking down glucose using oxygen in the form of adenosine triphosphate (ATP) by the process of catabolism.

At rest, a person requires a minimum amount of energy to perform the necessary biochemical processes in vital organs (such as heart, kidneys, liver etc.) for survival. This minimum expenditure of body is termed as the basal metabolic rate and the amounts to about 70 % of the daily energy expenditure in most sedentary individuals. Basal metabolic rate is different for each individual depending on differences in body size and amount of skeletal muscle. Total metabolic heat generated is the sum of the basal metabolic heat and any additional heat generated during thermoregulation [19].

$$Q_m = Q_{m,bas,0} + \Delta Q_m \quad (3)$$

The change in basal metabolic heat generation is influenced by the dependency of biochemical processes on local tissue temperature. In thermal physiology this is modelled according to the Q_{10} -effect, which states that for every 10 °C rise in temperature there is a corresponding increase in basal metabolism. In muscles metabolism variation is induced either in terms of exercise (dependent on the intensity) and/or muscular contractions caused by shivering [25]:

$$\Delta Q_m = \Delta Q_{m,bas} + Q_{m,sh} + Q_{m,w} \quad (4)$$

with, $\Delta Q_{m,bas} = Q_{m,bas,0} \cdot \left[Q_{10}^{(T-T_0)/10} - 1 \right] \quad (5)$

where, $\Delta Q_{m,bas}$ is the change in thermoneutral and normal basal conditions, metabolic heat generated by shivering is denoted by $Q_{m,sh}$ and $Q_{m,w}$ is the heat contribution from exercise. In equation (5), Q_{10} refers to the sensitivity coefficient which is generally equal to

2 [19], meaning for every 10 °C rise in temperature the basal metabolic heat generation doubles.

Blood perfusion

Metabolic processes continually require glucose and oxygen which are transported to the cells through blood. This dependency on blood directly affects the metabolic heat generation in tissue. The main blood vessels are the arteries and the veins. As these blood vessels reach the extremities of the body, many smaller blood vessels branch off to perfuse the organ, muscle, fat and skin tissue shown in Figure 6 (a). Blood perfusion represents the local blood flow through the capillary network and extracellular spaces in the tissue. The heat exchange between blood and perfused tissue is dependent on the local tissue temperature T and the blood temperature T_{artery} . To characterize heat transfer tissues, the Pennes' bioheat equation (1) from Chapter 2 is used, which is reproduced by the classical equations of heat diffusion that consider various material properties and geometry of the tissues from body elements. The equation describes the influence of homogeneous distributed blood flow on the temperature distribution in the tissue [7].

- $\rho c \frac{\partial T}{\partial t}$ - Transient term
- $\nabla k \nabla T$ - Spatial diffusion term, temperature variation over the physical geometry
- $\rho_b c_b \omega_b (T_{\text{artery}} - T) + Q_m$ – Source term, Heat generated due to perfusion of blood that is provided to the body part and basal metabolic heat

The blood perfusion term assumes that heat is exchanged with the tissue in the capillary bed and heat is not stored in the blood stream.

Heat Conduction

The metabolic heat generated in the cells is transferred to the surroundings through conduction. This is a type of sensible heat transfer, meaning heat transfer takes place due to presence of thermal gradient between the source and the surrounding. Heat conduction is the direct translation of heat energy, where heat flows from a hot body to a cold body. This heat flow is defined by the heat flux q_{cond} . From the heat conduction equation (6) also

known as Fourier's law. The heat flux is directly proportional to the temperature gradient. The proportionality constant is a material parameter, the thermal conductivity κ .

$$q_{cond} = -\kappa \frac{\partial T}{\partial x} \quad (6)$$

3.1.2 External heat transfer

Heat flow from inside the body takes place when the body surface is at a lower temperature than the core. The fact that the internal temperature is maintained at around 37 °C indicates that there is balance of heat exchange between the human body and its environment. In case of an imbalance between the amount of heat generated and the heat lost, heat transfer to the environment is limited despite heat exchanges within the body. As a result, heat generated would then be stored and body temperature would rise about 1 °C per hour for a resting person [5].

For the passive system, it is considered that the heat generated inside the human body is balanced instantaneously by the various heat losses due to convective, radiative and evaporative heat transfer as shown in Figure 3. Although in practice the process is dynamic and not a stationary equilibrium, external conditions change, so the body responds to 'regulate' the internal body temperature by acting upon feedback signals. Thermoregulation is further discussed with respect to the active system in next section.

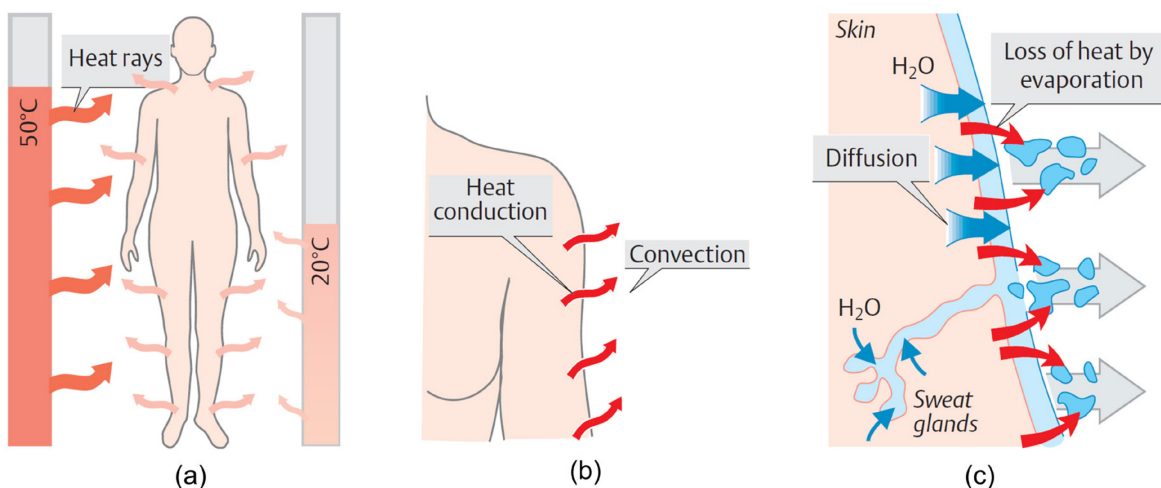


Figure 3: Heat loss mechanisms (a) Radiation, (b) Convection, (c) Evaporation [26]

Based on equation (2) a generalized heat transfer with the environment can be written as [19]:

$$q_{sk} = q_{rad} + q_{conv} + \dot{E}_{skin} \quad (7)$$

where, q_{sk} is the total heat transfer between the skin surface and the environment q_{rad} , q_{conv} and \dot{E}_{skin} are the radiative, convective and evaporative heat transfer per unit area respectively.

Murakami et al. [27] conducted a computational fluid dynamics (CFD) study to simulate heat and mass transfer from human body using a computational thermal manikin. A two-node thermal model was incorporated to perform a combined simulation in stagnant flow field. Total metabolic heat of about 100 W/m^2 was released in the environment through radiative, convective, evaporative and respiratory heat loss, associated results with respective contributions are presented in Table 2.

Table 2: Contribution of various heat transfer mechanisms towards heat loss [27]

Heat loss mechanism	Contribution to heat loss
<i>Radiation</i>	38,1 %
<i>Convection</i>	29,0 %
<i>Evaporation</i>	24,2 %
<i>Respiration</i>	8,70 %

Radiation

The process of thermal radiation is described by the Stefan-Boltzmann law of black-body-radiation. The heat loss is in the form of infrared rays in all directions, the amount of heat irradiated is highly dependent on the ambient temperature. In a cooler environment the heat loss from the body is high, whereas in a hotter ambient temperature there is a heat gain due to radiation. As the human body (skin) is not a perfect black body, the emissivity parameter leads to a description of a grey body. The Stefan-Boltzmann law states, heat radiated per unit surface area:

$$q_{rad} = \sigma \varepsilon F (T_{skin}^4 - T_{amb}^4) \quad (8)$$

with the Stefan-Boltzmann constant $\sigma = 5.6705 \times 10^{-8} \text{ W}/(\text{m}^2 \text{ K}^4)$, emissivity ε typically about 0.95 [5] and F is the view factor that factors the radiation from the radiative surface to the radiated surface, for a nude human this value is one. Radiation is a major contributor towards the heat loss to the environment accounting for about a third of the total expenditure.

Convection

The removal of heat from the skin surface by means of air currents takes place in the form of convection. Continuous heat loss through convection occurs as long as the ambient air temperature is below the skin surface temperature (i.e. $T_{skin} > T_{amb}$). The skin tissue heats the local air through conduction illustrated in Figure 3 (b). A small amount of natural convection is generally present around the body because the adjacent air rises away as it is heated. The thickness of the heated layer is determined by temperature differences and the environmental conditions, including air velocity. The convective heat transfer per unit area (W/m^2) is given by:

$$q_{conv} = h_c(T_{skin} - T_{amb}) \quad (9)$$

where, h_c (in $\text{W}/(\text{m}^2 \cdot \text{K})$) is the convective film coefficient.

When the body is exposed to wind, the skin adjacent layer of air is replaced immediately by new air much more swiftly than normally, which in turn increases the amount of heat loss. A general formula for calculating the influence of velocity on the convective film coefficient based on previous experimental studies is given by equation (10) and (11) [28].

$$h_c = 8.3 v^{0.6} \quad \text{for } 0.2 < v < 4.0 \quad (10)$$

$$h_c = 3.1 \quad \text{for } 0 < v < 0.2 \quad (11)$$

where, v is the air velocity in m/s.

Evaporation

Change of state of water from liquid to vapour occurs with the help of latent heat which is extracted from the surface, this in turn cools the surface. In humans the evaporative heat loss takes place in two forms, sweating through skin and diffusion of water through skin.

This insensible evaporation through the skin and lungs during respiration takes place involuntarily and thus cannot be regulated as it takes place due to diffusion. As the heat loss through diffusion does not contribute as much as sweating, in the human thermal system evaporative heat transfer is given in terms of vapour pressures as:

$$\dot{E}_{skin} = h_e (P_{sk,s} - P_a) \quad (12)$$

where, h_e is the evaporative heat transfer coefficient, $P_{sk,s}$ and P_a are the saturated vapour pressure at skin temperature and partial vapour pressure respectively. The evaporative coefficient can be expressed in terms of the convection coefficient using the Lewis relation [5] :

$$\frac{h_e}{h_c} = 16.5 \frac{K}{kPa} \quad \text{in } \frac{K}{kPa} \quad (13)$$

Relative humidity, ϕ is:

$$\phi = \frac{P_a}{P_{sa}} \quad (14)$$

The Antoine's equation for the saturated vapour pressure, P_{sa} and saturated vapour pressure at skin temperature, $P_{sk,s}$:

$$P_{sa} = 0.1 \exp\left(18.956 - \frac{4030.18}{T_{amb}+235}\right) \quad \text{in kPa} \quad (15)$$

$$P_{sk,s} = 0.1 \exp\left(18.956 - \frac{4030.18}{T_{skin}+235}\right) \quad \text{in kPa} \quad (16)$$

Finally, the evaporative heat loss in W/m^2 can be expressed as:

$$\dot{E}_{skin} = 1.65 h_c w \left[\exp\left(18.956 - \frac{4030.18}{T_{skin}+235}\right) - \phi \exp\left(18.956 - \frac{4030.18}{T_{amb}+235}\right) \right] \quad (17)$$

here, w is skin wettedness which is the fraction of skin covered by sweat to be evaporated. Loss of heat by sweat evaporation is continuously regulated. This aspect is further discussed in the active system.

Respiration

Dry convective heat transfer takes place inside the lungs. During the respiratory cycle the cool air inhaled is heated by the higher temperature body core and exhaled into the environment [5]. The overall contribution of this heat loss mechanism is about a tenth of the total heat transfer. Along with heat, mass transfer also takes place inside the lungs when the moisture of the inhaled air is increased. The respiratory heat loss is given by:

$$E_{res} + C_{res} = [0.0014 M(34 - T_{amb}) + 0.0173 M(5.87 - P_a)] \quad (18)$$

where, M is the metabolic heat generation in W/m^2 .

Another name for respiratory heat loss is ‘Panting’ which is more noticeable in animals which have their body surfaces covered in fur and lack sweat glands, which restricts most of the evaporative heat loss [25].

3.2 The active human thermal system

As discussed in previous sections, human body has a natural tendency to maintain the body core temperature at 37°C with the help of continuous heat exchange with the environment. Whenever a change in the environment takes place, a thermal imbalance in heat transfer is stimulated. Thermoreceptors in the form of nerve fibers, spread across the body, sense this variation and send the appropriate signal back to the hypothalamus (a part of the brain). The hypothalamus operates on a complex feedback temperature control system with multiple inputs to maintain a balance between internal and external heat transfer [19].

For normal human operation, it is important that the internal core temperature changes as little as possible despite fluctuations in the surrounding environment. The core temperature is the set point which needs to be maintained, the detectors (in this case the thermoreceptors) measure the system variable (temperature of the regulated part) and compare it against the threshold values. The correctional mechanism (blood perfusion, metabolism, etc.) then operates on this feedback to achieve the set point value. Cold and hot conditions have a large effect on the various heat loss mechanisms. At low temperatures heat transfer due to radiation is the maximum, whereas in hot environments above 30°C the evaporative heat loss due to sweating is the dominant mechanism of heat

transfer. This can be better visualized in Figure 4. The thermoregulatory system operates three major mechanisms: shivering (at low skin and core temperatures), sweating (at higher skin and core temperatures), and vasomotor response (comprising of vasodilation and vasoconstriction of blood vessels). A representation is shown in Figure 5.

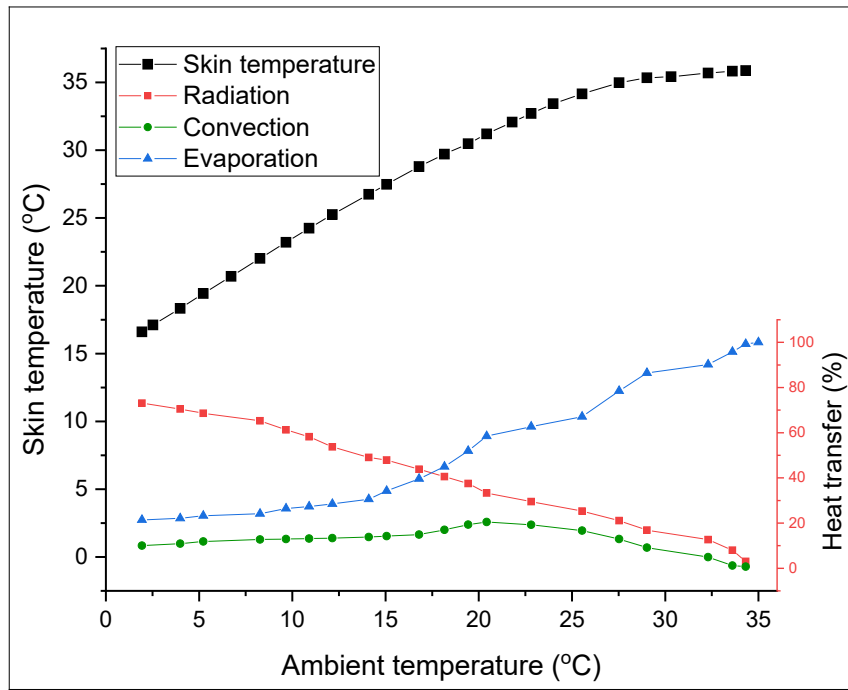


Figure 4: Variation in heat transfer mechanisms with temperature [29]

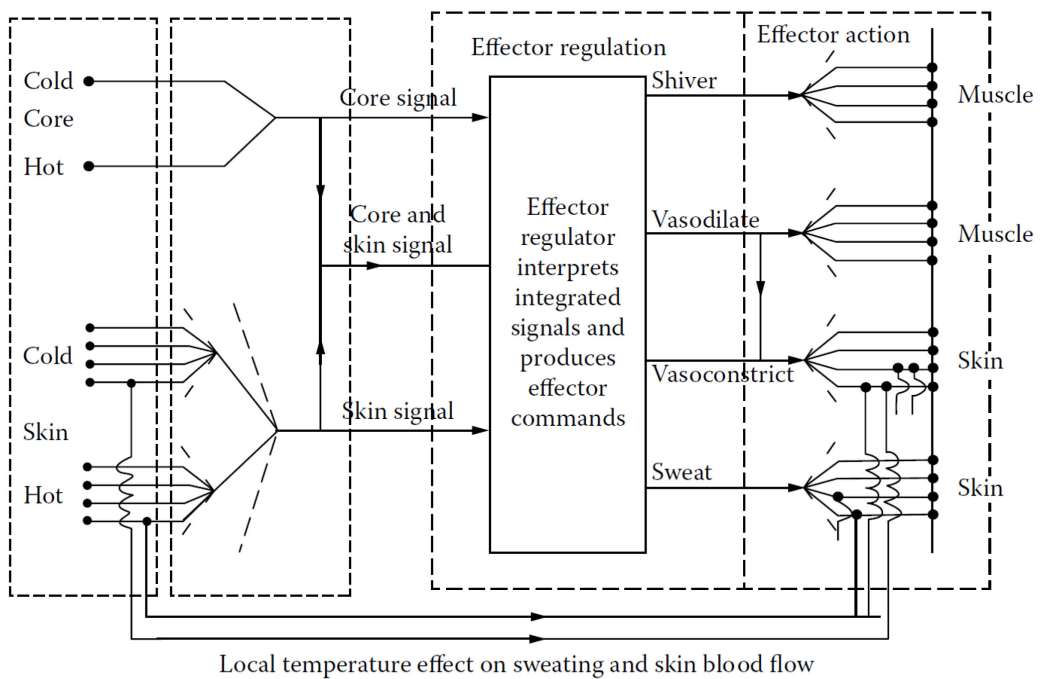


Figure 5: Representation of the active system of the Stolwijk's 25-node model [15]

3.2.1 Shivering

Shivering is one of the most effective tool with the help of which the body generates heat quickly. Onset of shivering is triggered due to the lowering of skin and core temperatures, typically as a result of exposure to cold temperatures. Shivering leads to an increased muscle tone as a result of microactivity in the skeletal muscles, thus significantly increasing the metabolic heat generation by up to five times without any external work [5]. The amount of metabolic heat generated as a result of shivering is dependent on the core and skin temperatures, based on the Gagge's two-node model, the following relation is often used [12]:

$$M_{shiv} = 19.4 C_{SIG_{sk}} C_{SIG_{cr}} \quad (19)$$

where, $C_{SIG_{skin}} = (33.7 - T_{skin})$ and $C_{SIG_{core}} = (36.8 - T_{core})$. These present the threshold for skin and core temperatures below which thermogenesis is initiated in the model and M_{shiv} is the metabolic heat generation in W/m^2 .

3.2.2 Vasomotor response

Blood travels from the heart to the skin surface via the cardiovascular system, heat is transported along with the essential nutrients. The major arteries branch into narrow arteriole and then further divide into small capillaries that are spread across the tissue. These capillaries then rejoin to form venule and then subsequently merge to become veins that recirculate back to the heart (Figure 6, (a)) [25]. The proximity of capillaries close to the skin surface plays an important role in heat exchange with the environment. Due to the fact that blood is continually circulated across the body, it is important to regulate the amount of blood flow through these capillaries. As the ambient temperature changes, the amount of heat transfer with the environment from the blood vessels should change as well. The thermoreceptors across the body sense the change in temperature and signal the hypothalamus to take the appropriate action in the form of dilating (increasing vessel diameter) or constricting (decreasing vessel diameter) the blood vessel (Figure 6, (b)), thus changing the amount of blood flow and subsequently the heat transfer through the vessels.

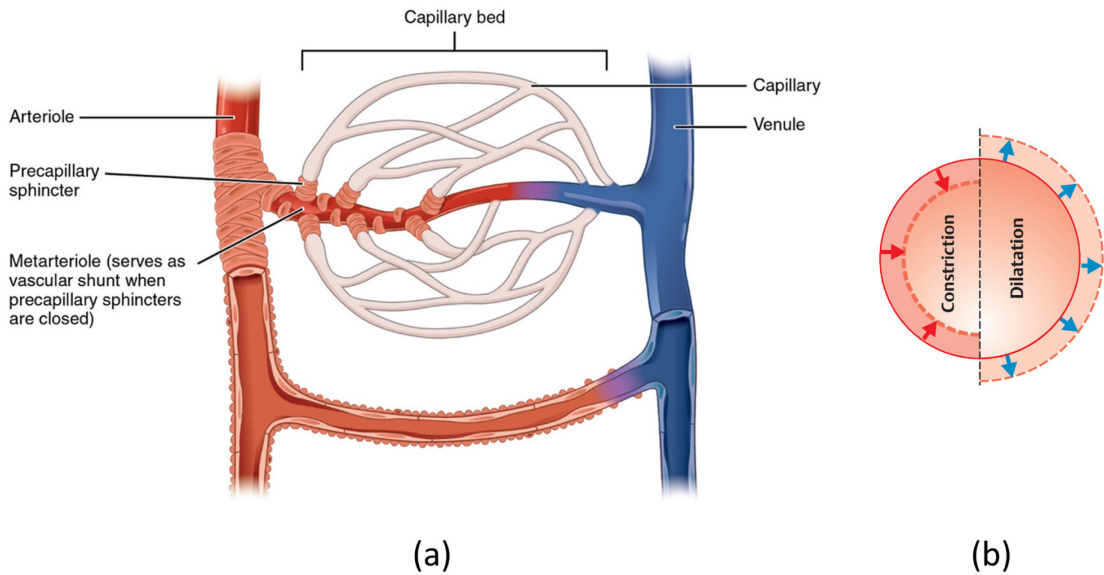


Figure 6: (a) Capillary bed showing the branching of blood vessels [30], (b) Change of blood vessel diameter in case of vasoconstriction and vasodilation [26]

Vasoconstriction

In case of exposure to cold temperature, the primary goal of the thermoregulatory system is to maintain the core temperature by minimizing heat loss to the environment. This is done by reducing the internal diameter of the blood vessels which reduces the blood flow rate in the capillary bed. The vessel diameter is small enough to allow a small amount of oxygenated blood essential for the cells. Vasoconstriction effects are prominent in the skin layer and are also observed in localized regions, the muscular blood flow is unaffected by short term thermoregulatory responses. As the skin is separate from the body core, the insulating properties of the fat layer help in preventing undesirable heat transfer. Fiala et al. in 2001 performed multi-linear regression analysis to calculate the vasoconstriction signal [21], the control equation generated for C_s was:

$$C_s = 35 [\tanh(0.34 \Delta T_{sk,m} + 1.07) - 1] \Delta T_{sk,m} + 3.9 \Delta T_{sk,m} \frac{dT_{sk,m}}{dt} \quad (20)$$

where, $T_{sk,m}$ is the mean skin temperature. This constriction signal is then used to calculate skin blood flow in terms of energy equivalent terms, more information is available in [21].

Vasodilation

In conditions where the core temperature rises above a threshold of 37.2 °C, counter reflex to the thermoregulatory response during vasoconstriction takes place. The inner diameter of blood vessels is enlarged to allow excess heat to be released to the environment. The larger diameter enables an increased skin blood flow. Similar to constriction signal, a dilation signal was also presented by Fiala [21]:

$$Dl = 21 [\tanh(0.79 \Delta T_{sk,m} + 0.70) + 1] \Delta T_{sk,m} + 32 [\tanh(3.29 \Delta T_{hy} - 1.46) + 1] \Delta T_{hy} \quad (21)$$

where, T_{hy} is the hypothalamus temperature.

3.2.3 Sweating

At higher ambient temperatures when the core temperature rises above the sweating threshold, sensible heat loss has very little to no contribution towards over all heat transfer as observed in Figure 4, thus evaporation through sweating is a crucial cooling mechanism for heat loss. From Section 3.1.2, the evaporative heat loss is governed by equations (12-17). Skin wettedness, w has a direct effect on the rate of evaporation, the value of w is between 0.06 (natural diffusion of water) and 1 (completely wet skin) [5]. When the skin is completely wet, maximum evaporative heat transfer takes place, if the rate of sweat secretion is more than the amount evaporated ($w > 1$), the excess water drips over the skin as it cannot evaporate, thus not contributing towards heat loss. Other factors affecting the rate of evaporation are relative humidity, ambient temperature and amount of physical activity etc.

3.3 Thermoelectric generators

Thermoelectric generators are solid-state devices that enable conversion of thermal to electrical energy. Figure 7 shows the setup of a typical TEG. The assembly is made from an array of thermocouples consisting of p-type (hole transporting) and n-type (electron transporting) semiconductor elements. These are connected electrically in series with

copper interconnects. The thermocouples are thermally connected in parallel between two ceramic plates [31].

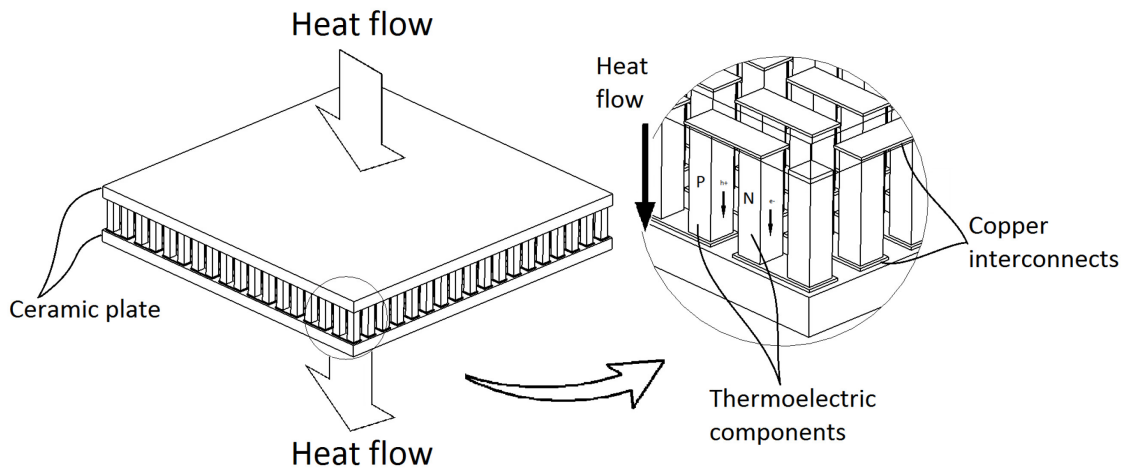


Figure 7: TEG with ceramic plates, thermocouples and copper interconnects

The energy conversion in a thermocouple is based on the Seebeck effect, where a temperature difference drives charge carrier diffusion towards lower temperatures. This results in a potential difference across the thermocouple. The magnitude of the voltage output from equation (22) is proportional to the difference of the Seebeck coefficients α_1 and α_2 , number of semiconductor thermocouples n and the temperature difference ΔT . The maximum power delivered into a load resistor can be calculated using equation (23) with R_{el} as the internal resistance of the TEG [32].

$$V_{out} = n \cdot \Delta T (\alpha_1 - \alpha_2) \quad (22)$$

$$P_{max} = \frac{V_{out}^2}{4 R_{el}} \quad (23)$$

The performance of thermoelectric modules is measured with a dimensionless quantity, figure of merit (ZT) given by equation (24). To obtain a high value, both Seebeck coefficient (α) and electrical conductivity (σ) should be increased, whereas thermal conductivity (κ) shall be minimized. For a thermoelectric device with two semiconductor materials [33], the figure of merit is calculated using equation (25) where, ρ is the electrical resistivity and the respective material properties of p-type and n-type material are used.

$$ZT = \frac{\sigma \alpha^2 T}{\kappa} \quad (24)$$

$$ZT = \frac{(\alpha_p + \alpha_n)^2 \bar{T}}{[(\rho_n \kappa_n)^{1/2} + (\rho_p \kappa_p)^{1/2}]^2} \quad (25)$$

Most commercially available thermoelectric devices use doped semiconductors with large values for the Seebeck coefficients (p-type: 2×10^{-4} (V/K), n-type: -2×10^{-4} (V/K)). Material properties of the semiconductors are temperature dependent. For room temperature applications bismuth telluride is used with a typical ZT value ranging from 0.8 to 1.0. For the top and bottom plates of the TEG, ceramic aluminum oxide (96 % purity) is used showing high electrical resistivity (10^{14} Ωm) and low thermal conductivity (25 W/(m K)). Interconnects between the p- and n-type semiconductors are made using copper with high thermal conductivity (400 W/(m K)) and low electrical resistivity (1.68 Ωm).

4 Simulation methodology

In this chapter, simulations of the passive and active human thermal system for different geometries of the human body are studied using the developed computational method in the finite element analysis (FEA) tool ANSYS Mechanical 19.0. The simulations were performed on a Dual Intel(R) Xeon(R) CPU E5-2680 v3 @ 2.50GHz with 128 GB RAM on 16-core Distributed Memory Parallel. ANSYS Parametric Design Language (APDL) scripts are used for implementation of certain physiological processes for numeric calculation. These scripts calculate heat transfer contributions of different terms (such as heat generation due to blood perfusion and evaporative heat loss) for simulating the human thermal system. Furthermore, this chapter details the sequence of steps utilized for model development. Subsequent results are discussed in Chapter 5.

In the first part of this chapter, stationary thermal simulations for the passive system of four different human tissue geometries are performed to evaluate the temperature distribution. Model details include Pre/Post processing of geometry, mesh details, analysis settings and boundary conditions. While the second part presents the steps taken to perform the transient simulations for the thermoregulatory control loop. A proportional control loop is applied on the cubic tissue geometry and response for perfusion, metabolic heat generation and sweating rate is analyzed.

4.1 Stationary heat transfer in humans

It is necessary to establish an understanding of how the passive system behaves under thermoneutral conditions before considering the transient thermoregulatory effects. A series of stationary thermal analysis are performed in this work with increasing complexity. The physical effects are defined based on the definitions in Chapter 3. The heat-transfer processes are categorized into two parts: internal heat transfer and external heat transfer. Thermal properties of the biological tissues are defined for realistic implementation of these processes. In each model, the equations are solved for different types of human tissues. Muscle, subcutaneous fat and skin tissue form the fundamental layers for every model. More complex models such as the torso includes additional complex tissues like bones, blood vessels, cartilage and vital organs. Standard thermo-physical properties of

tissues are not widely consistent across literature. For present analysis, the material properties are taken from the database maintained by IT'IS Foundation [34], a non-profit and independent research organization. The properties have been drawn from a comprehensive scientific literature review. It is understood that for some material parameters, such as blood perfusion, the variation in values can be large, which in turn can have a severe effect on simulation results. The database presents the averaged thermal properties across the number of studies with maximum and minimum values. Table 3 lists the average thermal properties for each tissue used. Additional model specific physiological properties such as the metabolic heat generation and heat transfer rate are presented in Table 4.

Table 3: Average thermal properties of tissues from the IT'IS database [34]

Tissue	Density	Specific heat	Thermal conductivity
	$\rho, (\text{kg}/\text{m}^3)$	$c, (\text{J}/(\text{kg K}))$	$\kappa, (\text{W}/(\text{m k}))$
Blood	1049.75	3617.0	0.516
Bone (Cortical)	1908.00	1312.8	0.320
Bone Marrow (Red)	1028.50	2666.0	0.279
Cartilage	1099.50	3568.0	0.487
Heart Muscle	1080.80	3686.0	0.557
Kidney	1066.25	3763.0	0.534
Large Intestine	1088.00	3654.5	0.542
Liver	1078.75	3540.2	0.519
Lung	394.00	3886.0	0.387
Muscle	1090.40	3421.2	0.494
SAT (Subcutaneous Fat)	911.00	2348.3	0.211
Skin	1109.00	3390.5	0.372
Spinal Cord	1075.00	3630.0	0.513
Stomach	1088.00	3690.0	0.525
Trachea	1080.00	3568.0	0.487
Urinary Bladder Wall	1086.00	3581.3	0.522
Uterus	1104.50	3676.0	0.526

Table 4: Averaged and minimum value for metabolic heat generation and perfusion rate [34]

Tissue	Heat Generation Rate (W/m ³)		Heat Transfer Rate (1/s)	
	Average	Minimum	Average	Minimum
Blood	0.0000	0.0000	0.174958	0.174958
Bone (Cortical)	295.4899	295.4899	0.000318	0.000318
Bone (Cancellous)	547.4617	182.4872	0.000589	0.000196
Bone Marrow (Red)	2150.3164	1592.8270	0.002314	0.001714
Cartilage	595.9744	595.9744	0.000641	0.000641
Heart Muscle	42640.2028	25311.7787	0.018483	0.010972
Kidney	19247.6864	13221.4092	0.067441	0.046326
Large Intestine	12893.9525	5644.6628	0.013876	0.006075
Liver	10712.8928	5254.0017	0.015470	0.007587
Lung	2446.4143	434.9181	0.002633	0.000468
Lung (Deflated)	6519.6319	1159.0457	0.007016	0.001247
Muscle	988.0384	498.5245	0.000668	0.000337
SAT (Subcutaneous Fat)	461.4816	279.8010	0.000497	0.000301
Skin	1827.0953	841.5733	0.001966	0.000906
Spinal Cord	2669.2951	2164.2933	0.002873	0.002329
Stomach	7756.3121	1782.5251	0.008347	0.001918
Trachea	585.4046	585.4046	0.000630	0.000630
Urinary Bladder Wall	1311.8637	1311.8637	0.001412	0.001412
Uterus	7825.6626	2907.8965	0.008422	0.003129

As in all modelling processes, complex systems must be simplified in order to have a balance between a desired accuracy in results and associated computational costs. For simplicity only the thermal system for heat transfer is analyzed, though a coupled simulation between thermal and fluid (blood) systems can be performed to obtain a more comprehensive model.

To construct a realistic while still solvable model, some basic assumptions are made:

- blood flow not considered, resulting in constant values of blood perfusion in tissues;
- where applicable, temperature of blood vessels is fixed at 37 °C;

- all tissue materials are isotropic, there is no significant differences between the molecular composition of the body elements;
- biological response of the tissues like blood perfusion and basal metabolic heat generation rate is modelled using Pennes' bioheat equation (1);
- metabolic heat generation is applied to the entire solid tissue structure and modelled without Q_{10} -effect.

Additional model specific assumptions are discussed in further subsections.

Simulation setup

For setting up the physical environment, a standard approach of modelling is followed. As visualized in Figure 8, the process starts with the input data, this includes the material properties, geometry of the tissue and various parameters necessary for the definition of boundary conditions.

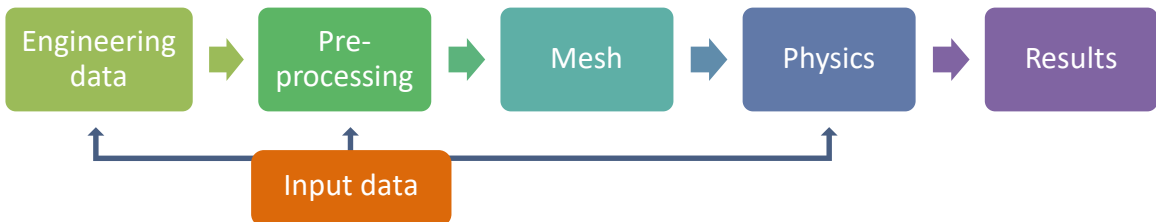


Figure 8: Process flow of simulation setup

First stage deals with the engineering data e.g. material parameters like specific heat or density, etc. The data for the material properties is taken from the IT'IS database based on Table 3. The second step is the geometry which represents the computational domain on which analysis is to be performed on. The geometry is then discretized into a finite number of sub regions to form the solution grid (mesh) for which the associated system of equations are solved. The simulation environment is prepared with boundary conditions and the analysis settings, an appropriate solver is selected for solving the system of simultaneous equations. The results obtained are then post processed to enable visualization of data, in the form of contour plots of temperature distribution, temperature plots along a path, etc. [35].

Bioheat equation

In the human body, blood flow plays an important role for heat transfer in biological tissue. The blood is pumped by the heart all over the body, from the core to the extremities through macrocirculation and microcirculation. The cardiovascular system comprises of large blood vessels that branch out first into smaller blood vessels and then into the capillary bed. The capillary bed acts as a homogenous structure due to the high density of small blood vessels (capillaries). The blood perfusion effects are the largest in these regions, this translates to the assumption that the blood perfusion and metabolic heat generation effects are modelled for the whole volume of the tissue. For performing the stationary simulations the steady state form (equation (26)) of the Bioheat equation was used:

$$0 = \nabla \kappa \nabla T + \rho_b c_b \omega_b (T_{\text{artery}} - T) + Q_m \quad (26)$$

The heat exchange between the blood and the tissue is dependent on the local tissue temperature and the blood temperature, which leads to heating of the tissue. The density of blood and specific heat give the amount and capacity of heat that can be transported. For the steady state analysis, values for the basal metabolic heat and perfusion rate was assumed to be constant without affecting the accuracy of the model.

To model these blood perfusion effects in ANSYS mechanical, APDL scripts are used. A sample command snippet is presented in Table 5, where total heat from the bioheat equation is applied as an elemental load on the specific tissue type. Values are defined by a special array type called table with which the solver calculates the heat generation for each element [35].

Tables allow application of varying loads and properties in scenarios where normally only constant load can be applied, values are calculated for each element of the target body through linear interpolation. Figure 9 shows the dependency of the heat generation load on temperature and between 37 °C and 15 °C the heat generation value is linearly interpolated and beyond 37 °C a constant basal metabolic heat generation is applied.

Table 5: APDL command for the bioheat implementation as heat generation load

```

!material properties of blood
rho = 1049.75          ! kg 1/m^3
c = 3617               ! J 1/kg 1/K
!perfusion rate and basal metabolic heat generation rate
omega_muscle = 0.000336873 ! 1/s
Q_muscle = 498.5245     ! W/m^3

!defines a table with TEMP as primary variable
*DIM,perfusionmuscle,TABLE,3,1,1,TEMP,

!TEMP values
perfusionmuscle(1,0,1) = 15
perfusionmuscle(2,0,1) = 37
perfusionmuscle(3,0,1) = 40
!HGEN values
perfusionmuscle(1,1,1) = (rho*c*omega_muscle*(37-15) +
Q_muscle)
perfusionmuscle(2,1,1) = (rho*c*omega_muscle*0. + Q_muscle)
perfusionmuscle(3,1,1) = (Q_muscle)

!apply the heat generation load to the elements of named
selection
cmsel,s,muscle
bfe,all,hgen,,%perfusionmuscle%
ALLSEL

```

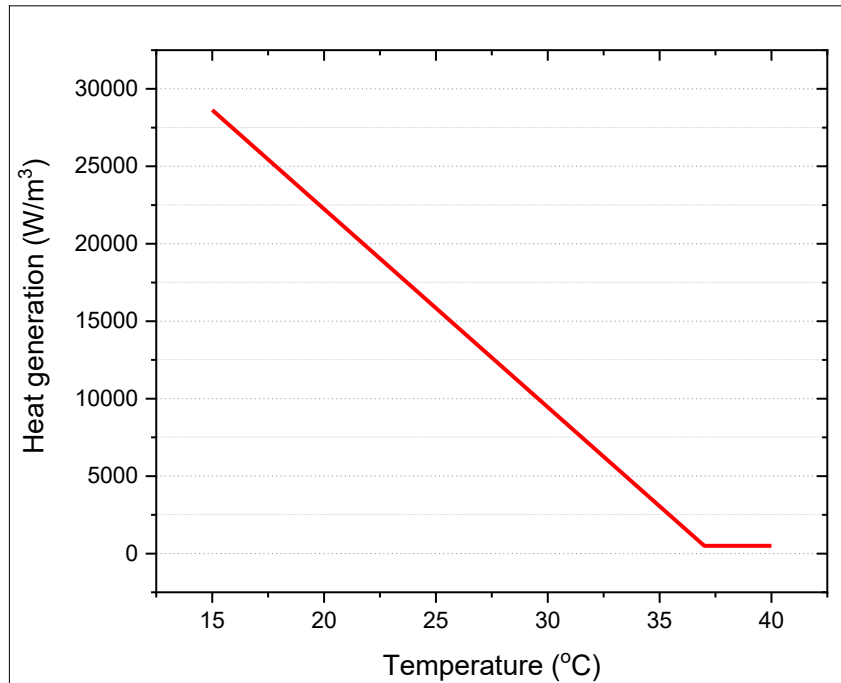


Figure 9: Table definition for temperature dependent heat generation based on Table 5

Heat conduction

For a steady state thermal analysis, ANSYS solves the system equation (27) for temperature T based on Fourier's law for heat transfer within a solid.

$$[K(T)]\{T\} = \{Q(T)\} \quad (27)$$

where, $[K(T)]$ is the heat transfer matrix, $\{Q(T)\}$ is the thermal load vector (heat flow) and $\{T\}$ is the unknown temperature vector [35].

Convective heat transfer

The convective heat transfer is applied on the outer surface of the skin layer for each model as the boundary condition 'Convection'. The amount of heat transfer is dependent on ambient temperature defined. It is assumed that there is no air flow over the skin surface ($v = 0$), therefore from equation (11) convective film coefficient value is taken constant at 3.1 W/(m² K).

Radiative heat transfer

As with convection, the radiative heat loss is also applied on the same skin surface as a separate boundary condition. The correlation property is specified as 'To Ambient', as all of the radiation energy is assumed to be exchanged with the surroundings at ambient temperature. The emissivity value is kept constant at 0.95 which is the typical value for the nude human body [5].

Evaporation

Evaporation is applied to the models as heat transfer in the form of heat flux moving out of the skin surface. From Chapter 3, it is apparent that the skin surface temperature plays an important role in the amount of heat that is taken away through evaporation, thus it is important to apply a temperature dependent heat flux in the same way as the bioheat equation is applied using tables in APDL. To capture the exponential nature of evaporative heat loss function (Figure 10); instead of three temperature values, 35 separate temperatures with corresponding heat flux values are defined as shown in Table 6.

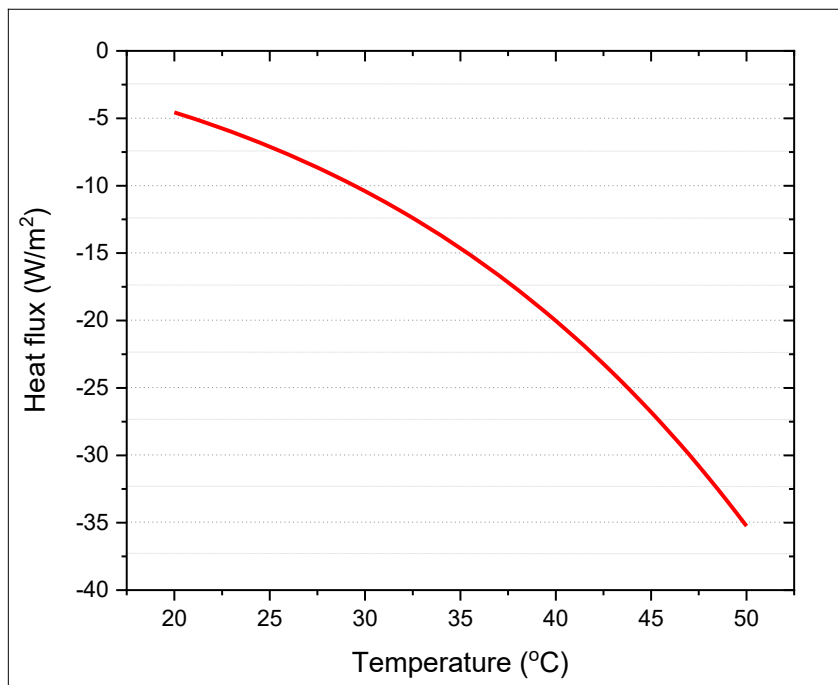


Figure 10: Table definition for temperature dependent evaporative heat flux

Table 6: APDL command for evaporative heat loss as heat flux

```

hc = ARG5      ! convection coefficient (3.1 W/m^2K)
ta = ARG6      ! ambient temperature (15 C)
phi = ARG7     ! relative humidity (0.5)
w = ARG8       ! skin wettedness (0.06)
*DIM, evap, TABLE, 35, 1, 1, TEMP,
!TEMP values
evap(1,0,1) = 20
.
evap(16,0,1) = 27.5
.
evap(35,0,1) = 37
!evap HFLUX
evap(1,1,1)= -(16.5*w*hc*0.1* ((exp(18.956-
(4030.18/(20+235))))-(phi*(exp(18.956-
(4030.18/(ta+235)))))))
.
evap(16,1,1) = -(16.5*w*hc*0.1* ((exp(18.956-
(4030.18/(27.5+235))))-(phi*(exp(18.956-
(4030.18/(ta+235)))))))
.
evap(35,1,1)= -(16.5*w*hc*0.1* ((exp(18.956-
(4030.18/(37+235))))-(phi*(exp(18.956-
(4030.18/(ta+235)))))))
!apply the heat generation load to named selection nodes
cmsel,s,skin_s
sf,all,hflux,%evap%

```

Human body geometry

The open-source MRI and CT imaging based human tissue model ‘*VHP-Female Version 2.2*’ [36–38] was created using the open-source high-resolution cryosection image dataset from the *Visible Human Project®* of the U.S. National Library of Medicine [39]. The model includes 26 individual tissues and 184 separate tissue parts in triangular surface mesh form which was converted to individual solid parts illustrated in Figure 11.

Pre-processing of the geometry is performed in ANSYS DesignModeler to separate each tissue type using boolean operations to generate a suitable geometry for thermal analysis in ANSYS Mechanical.

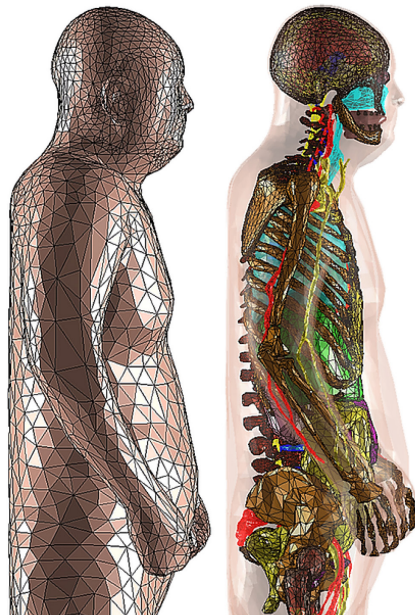


Figure 11: VHP-Female V.2.2 human model displayed in MATLAB environment [38]

4.1.1 Simplified cubic human tissue

The first model for the thermal simulation is chosen based on the work done by Yang et al. [6]. The model is a cubic geometry having a computational domain of $0.08 \text{ m} \times 0.08 \text{ m} \times 0.08 \text{ m}$. The geometry is divided into three layers: muscle, fat and skin tissues as shown in Figure 12, direction along x-axis denotes the tissue depth from the body core to the skin surface.

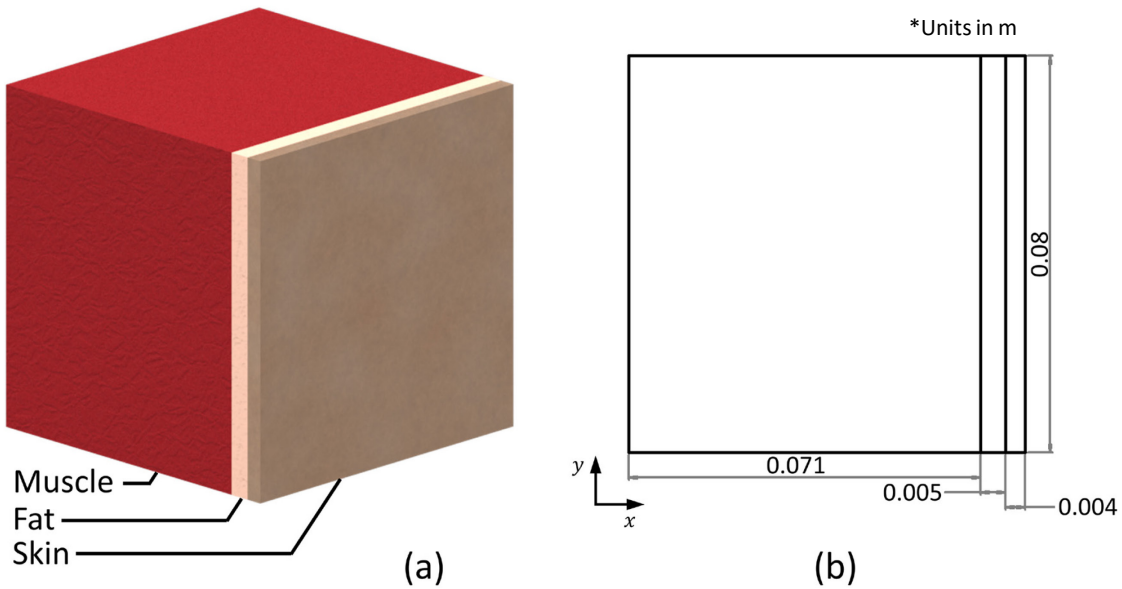


Figure 12: (a) The simplified human tissue model with muscle, subcutaneous fat and skin; (b) Dimensions of the model

As mentioned previously the tissue structures are considered isotropic, thus the thermal conductivity, specific heat, tissue density are uniform in each layer taken from Table 3. The model is tested against the averaged and minimum values of metabolic heat generation from the material database (Table 4). A structured grid is generated for the model, given its uniform shape, the mesh comprised of 65,525 nodes and 14,976 hexahedral elements as shown in Figure 13.

Boundary conditions

The environmental temperature along with initial temperature is kept at 15 °C. The skin surface is the main location where the heat transfer with the surroundings takes place. Convective, radiative and evaporative heat transfer mechanisms are defined as boundary conditions on this face. The film coefficient is kept constant at 3.1 W/(m² K), emissivity at 0.95 and evaporative heat transfer is defined as outward heat flux based on the command snippet in Appendix 8.1, Table 8. The rear face of the muscle layer is perfectly insulated (net heat flow is zero) as seen in Figure 13. The thermal contributions of all three biological tissues are evaluated based on the minimum values of metabolic heat generation and perfusion rates listed in Table 4. This thermal load is applied as a body force element (BFE) with the label heat generation (HGEN) as described in Appendix 8.1, Table 9.

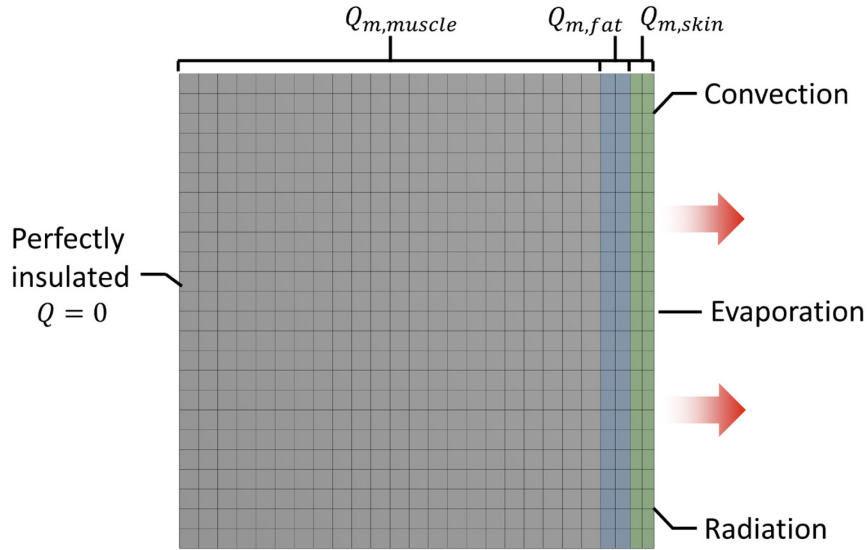


Figure 13: Hexahedral meshed model with boundary conditions

Analysis settings

A distributed sparse direct solver with substepping was selected because of the inherent nonlinearity of bioheat equation and radiation. Additionally, heat convergence is turned on with a tolerance of about 0.35 %, along with line search parameter. More details related to analysis settings are available in the Appendix, Figure 38.

4.1.2 Simplified human forearm

The cubic model presents a basic structure of the tissue. Though the model provides an understanding of heat transfer in the three basic tissue layers, influence of irregular structures such as bones and blood vessels on temperature distribution is not considered. To evaluate these effects, a simplified mockup of the human forearm is created. The geometry is prepared using concentric cylinders for muscle, fat and skin tissue, with off-center structures for bone and blood vessels (separate artery and veins) as illustrated in Figure 14. A structured grid is generated with 288,207 nodes and 69,249 elements for the model. Material properties for different tissues (muscle, fat, skin, blood vessels, blood and cortical bone) and minimum metabolic heat generation values are taken from Table 3 and Table 4 respectively.

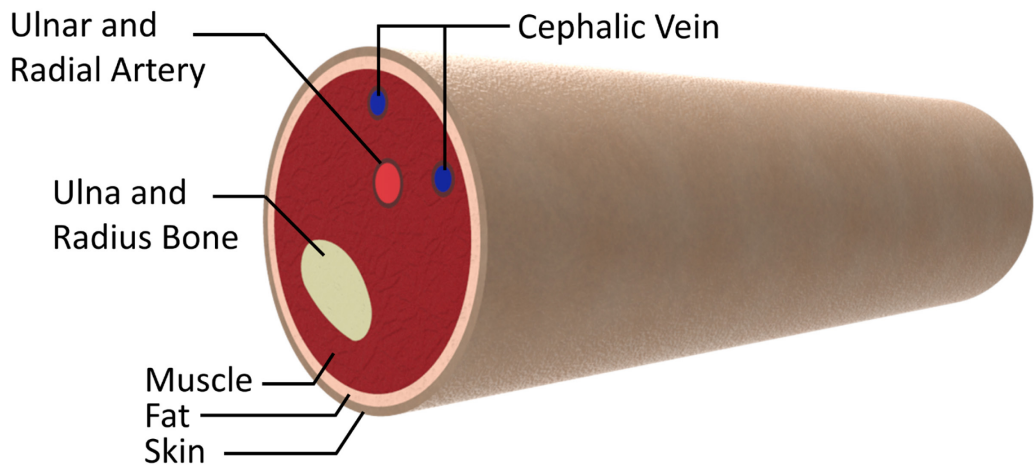


Figure 14: Simplified human forearm with muscle fat and skin along with blood vessels and bone

Boundary conditions and analysis settings

Similar to the previous model, the sensible and insensible heat losses were defined on the skin surface. To simulate the heat transfer from the blood through conduction, a dirichlet boundary condition of 37 °C is applied to the blood in artery and veins.

The simulations are performed at an ambient temperature 15 °C. Bioheat equation implementation is the same as the cubic model with perfusion and metabolic heat generation effects in muscle, fat and skin tissue. Program controlled heat convergence was turned on with a tolerance of 0.1 %.

4.1.3 Human forearm

The left human forearm is separated below the elbow from the human body geometry. This geometry strikes an ideal balance between complexity and size to test the implementation of the bioheat equation for realistic geometries.

Through boolean operations the muscle, fat and skin layers are separated, further boolean operation are performed to subtract the bones and blood vessels from the muscle geometry (Figure 15). The generated mesh consists of 104,295 nodes and 73,931 tetrahedral elements.

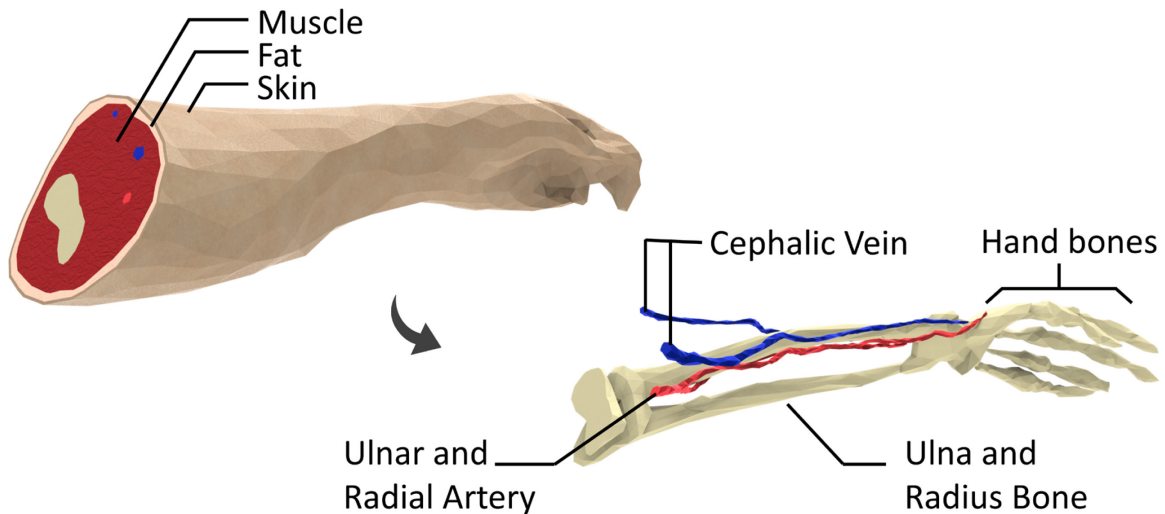


Figure 15: Human forearm model with internal bones and blood vessels

Boundary conditions and analysis settings

Figure 16 details the different boundary conditions applied to the model, as this is a faceted geometry named selections of different parts are made. A separate named selection of all 733 skin surface facets is made to apply the radiation, convection and evaporation. The artery and veins are fixed at 37 °C. The simulations are performed at different ambient temperatures ranging from 5 °C to 35 °C with a 5 °C increment. Bioheat equation implementation is same as previous models in muscle, fat and skin tissues based on minimum values.

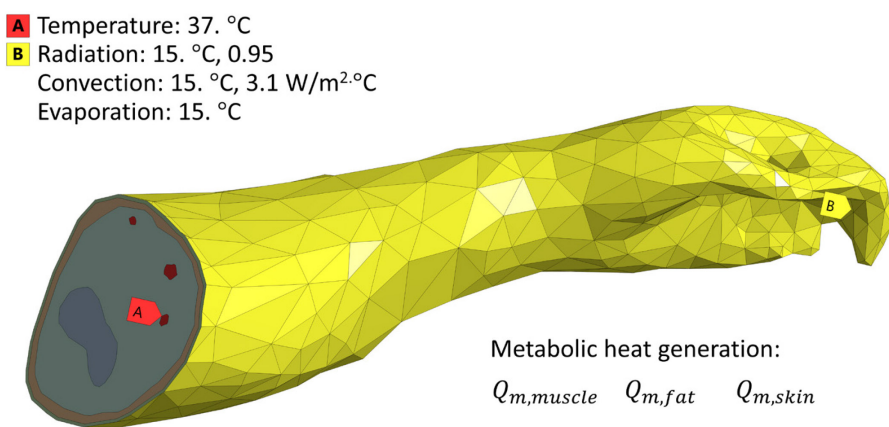


Figure 16: Boundary conditions for the human forearm at 15 °C

4.1.4 Torso

After successful analysis of the human forearm, simulations are performed on the most complex part of the human body: the torso. The model is comprised of 108 individual parts including the bones, cartilage, vascular network and internal organs, illustrated in Figure 17. The head, legs and arms are removed from the model to reduce the computational domain. Several boolean operations are used to subtract intersecting material between the muscle and other tissues. A computational grid of about 1.26 million nodes and 931,066 elements is generated.

Boundary conditions and analysis settings

Following the same methodology as the forearm, named selections are made for each category of tissue type along with a separate named selection for skin surface comprising 2,949 faces. Radiation, convective and evaporative surface loads are applied on the skin surface, with the blood vessels kept at 37 °C (Figure 18). The simulations are carried out for an ambient temperature of 15 °C. As stated in Section 4.1 the bioheat equation in tissues is implemented using a table, the calculated heat is applied as body force element (HGEN) to the whole tissue structure.

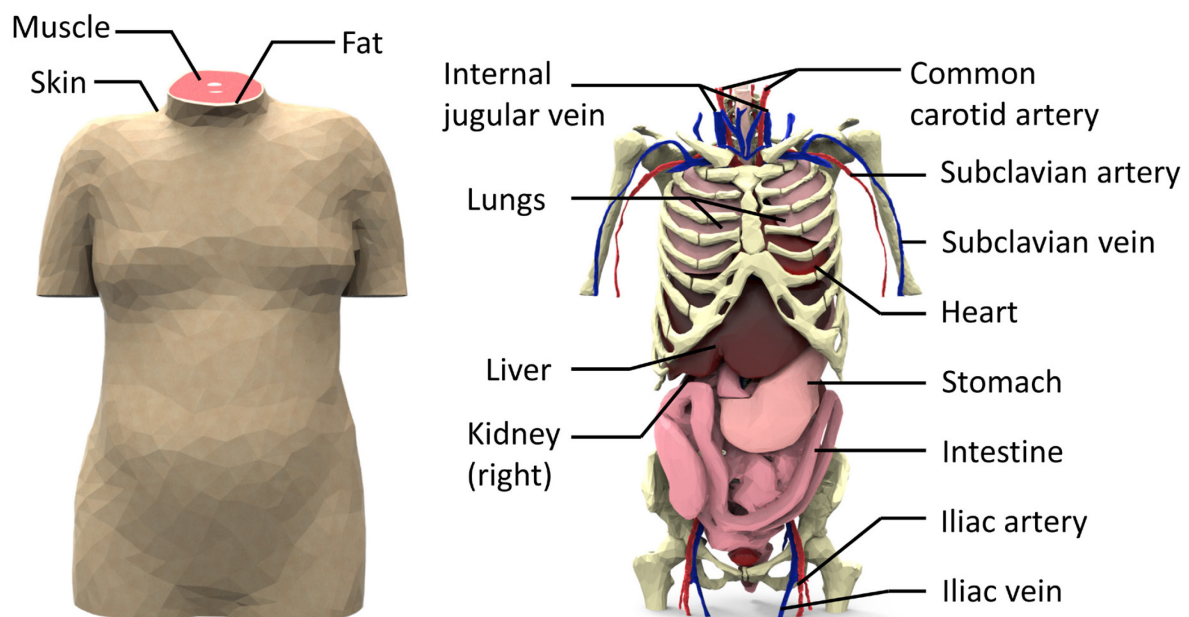


Figure 17: Human torso model with different tissue structures

The process works sufficiently well for previous models, but here blood perfusion implementation has been modified. Due to the way in which this geometry is developed, every part including the internal organs is a solid. The blood perfusion and metabolic heat generation rates for the internal organs such as the heart muscle, lungs, intestine etc. had to be adjusted using a factor for the thin wall volume to the shell volume ratio listed in Appendix, Table 12 . The application of HGEN is also shifted from elemental to nodal load on the surface of each organ (refer Appendix, Table 11). The blood perfusion and metabolic heat generation values for muscle, fat and skin are used same as the original elemental load applied to the entire volume. Given the complexity of the geometry and the irregularity between the different parts, to achieve convergence the heat convergence tolerance is increased to 0.5 %.

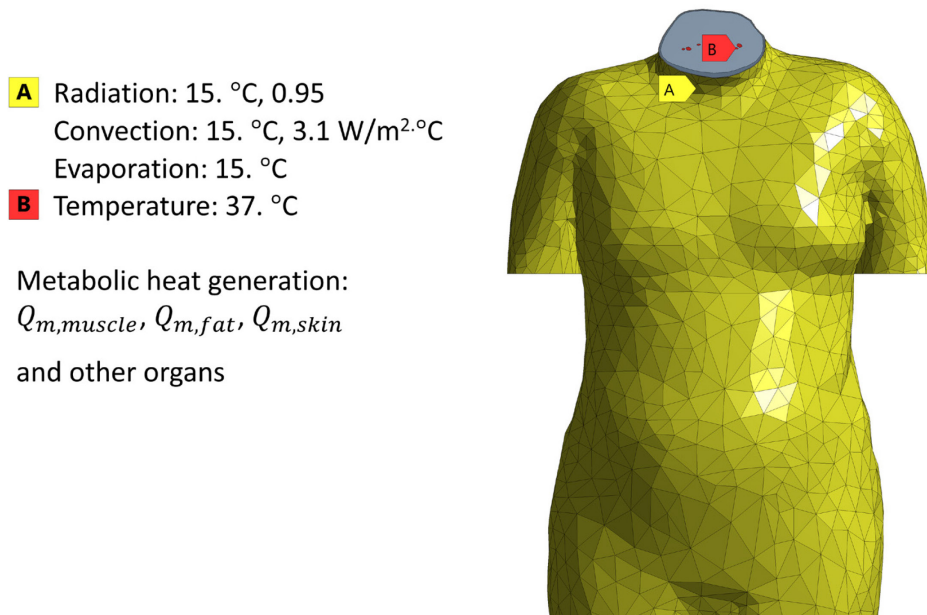


Figure 18: Boundary conditions for the human torso at 15 °C

4.2 Thermoregulatory control loop (Transient analysis)

The stationary simulations of the various tissue models provide a suitable starting point for introducing thermoregulatory response system. As established in Chapter 3, thermoregulatory reflexes are a part of the active thermal system that work towards maintaining the core temperature of the body at 37 °C. Thermoreceptors actively sense temperatures across the body and send the signal to the hypothalamus, which compares it against a set-point value. When a difference is detected, the effector mechanism sends

control signals to counter-balance the excess/deficiency in heat transfer. The regulatory mechanisms are in the form of shivering thermogenesis, sweating and vasoconstriction/dilation. These mechanisms have an effect on both the skin and the core temperature. The entire thermoregulatory system can be characterized as a multiple input control loop with continuous feedback gain. Many standard control systems can be implemented to mimic the basic procedure, such as, a basic control like an on-off (bang-bang) controller, proportional controller or a proportional–integral–derivative controller (PID), each with its merits and demerits.

Proportional control and implementation

For current implementation in ANSYS mechanical, a proportional controller is chosen, as an on-off controller has a tendency to oscillate around the set point value. In proportional control, the feedback signal is compared against a setpoint value, the instantaneous error, $e(t)$ is calculated between the two and the output signal, P_{out} is modified as a product of error and the proportional gain K_p .

$$P_{out} = K_p e(t) \quad (28)$$

A close loop controller is developed in the form of an APDL script and is tested on the simple cubic model (Figure 13). The present model operates based on the concept from Stolwijk [14] and skin blood flow equation from Fiala [21] (Q_{10} -effect was not modelled). The stationary simulation was used as the initial condition for the transient simulation under two ambient temperatures of 15 °C and 25 °C. Three separate proportional controllers regulate the perfusion rate in the muscle, sweat rate through skin wettedness and blood perfusion rate in skin as shown in Figure 19. The associated components for each controller are listed in Table 7. The command utilizes arguments (ARG) that allow manual definition of proportional gains and setpoint for the skin and muscle temperatures. The average temperature of the surface is calculated using a small subroutine and sent to the controller as the measured value. The associated command is attached in Appendix 8.1. Transient simulations were performed for 3,000 seconds with a fixed time-step of 30 seconds.

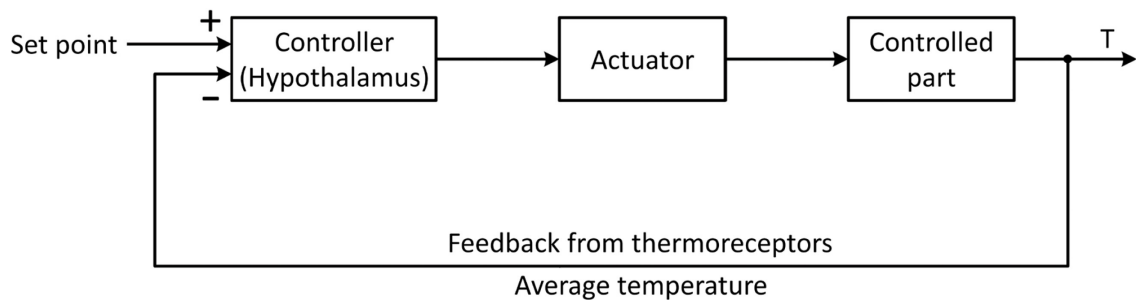


Figure 19: Control loop for current implantation of thermoregulation

Muscle

The setpoint for the back surface of the muscle is kept at 37 °C. The controller calculates the error between this measured value and the setpoint. Proportional gain of 5 is selected after a few trial simulations, this gain multiplies to the blood perfusion rate of the bioheat equation to give the output signal. This value is used as the new blood perfusion rate. To prevent accidental out-of-bounds value due to intensity of error, the blood perfusion rates are limited between maximum and minimum values taken from the database [34] using IF - ELSE conditional statements.

Skin

Two separate controllers are used on the skin layer, one to control the amount of blood flow and the other on the skin surface to control the amount of skin wettedness for evaporative heat loss. The setpoint for the skin surface is kept at 30 °C for ambient temperature of 15 °C and 35 °C for ambient temperature of 25 °C, and the feedback is taken from the average skin surface temperature. Proportional gain of 10 is used for both controllers. Onset of sweating is modelled by change in the skin wettedness coefficient.

Table 7: Components of the three controllers based on control scheme

Controller	Control action	Physiological action	Controlled part
I	Blood perfusion rate	Metabolic heat generation	Muscle
II	Blood perfusion rate	Vasoconstriction/-dilation	Skin
III	Skin wettedness	Sweating	Skin

The base value of 0.06 and a maximum wettedness of 1 were applied as limiters for the controller based on physiological data. Modelling vasomotor function is not a straightforward task, the experimental data for these values is scarce due to the inherent difficulty in measurement. Therefore, certain assumptions are made while modelling the skin blood flow. The skin blood flow equation without Q_{10} - effect based on Fiala model is used [40]:

$$\omega_{sk} = \frac{\omega_{sk,0}}{1+\alpha Bf} \cdot 2^{(T_{sk}-T_{sk,0})/10} \quad (29)$$

where, α is the distribution factor of tissue and Bf is the blood flow signal.

5 Results and discussion

This chapter presents the results obtained from the various simulations described in previous chapter. The output data is presented in the form of temperature distribution across the geometries of different models to present an understanding of how the heat is getting transferred across the tissue.

5.1 Stationary heat transfer in humans

5.1.1 Simplified cubic human tissue

This model provides an initial understanding of the influence of basic tissue types on the nature of heat transfer. Given to the low complexity of the model, the solution computed in 44 seconds. The following graph shows the temperature along a path on the central axis of the model simulated at an ambient temperature of 15 °C. The fat layer is marked between the two vertical lines.

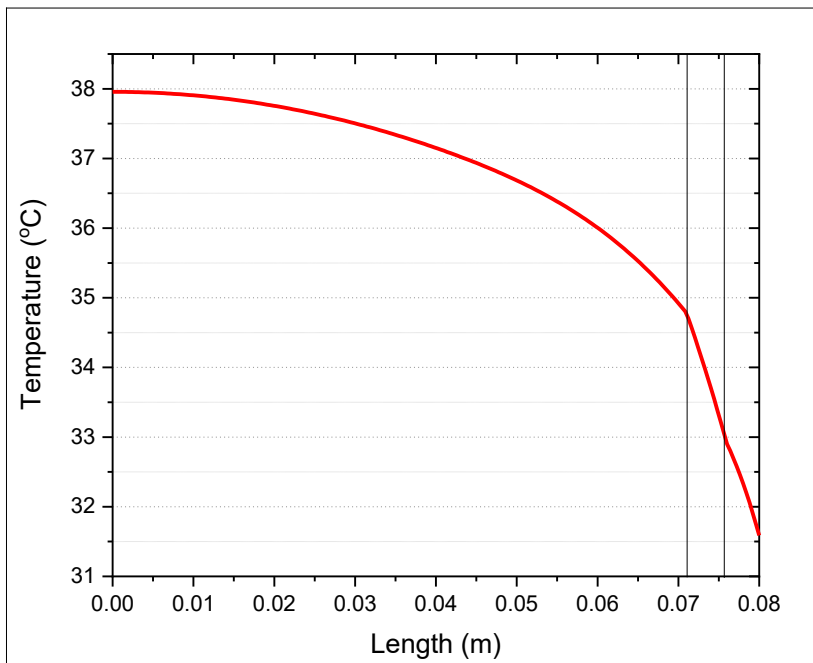


Figure 20: Temperature distribution along central axis of simplified cubic human tissue

It can be observed from the graph that the temperature decreases as we move away from the body core towards the skin surface. Also noticeable is the steep temperature drop of about 1.6 K in the fat layer. This can be attributed to the insulating property of fat inside the human tissue. Additional contour plot of the temperature distribution is available in Appendix 8.4, Figure 39. The temperature at the rear surface (core) of the muscle is at 37.9 °C and at skin surface is about 31.5 °C. The bioheat equation is implemented as a heat generation load (W/m^3) for the muscle, fat and the skin layers, thus the higher than normal core temperature could be a result of the relatively thick (0.071 m) muscle layer. To prevent this, the model could be modified to incorporate physiologically accurate dimensions for the muscle.

5.1.2 Simplified human forearm

The simplified human forearm presents a model with additional tissue types, like bones and blood vessels in a cylindrical layered structure. A dirichlet boundary condition of 37 °C is applied on the blood vessel bodies with ambient temperature of 15 °C. The solution completed in 1 minute and 50 seconds. Figure 21 presents the temperature contour on the model and from Figure 22, we can see the temperature profile along the path specified.

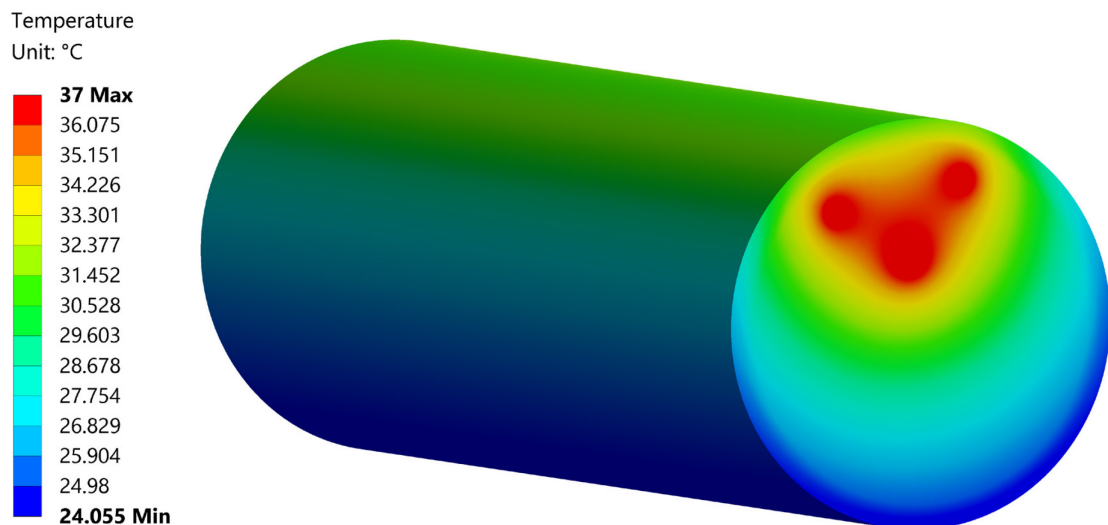


Figure 21: Contour plot of temperature distribution on simplified human forearm

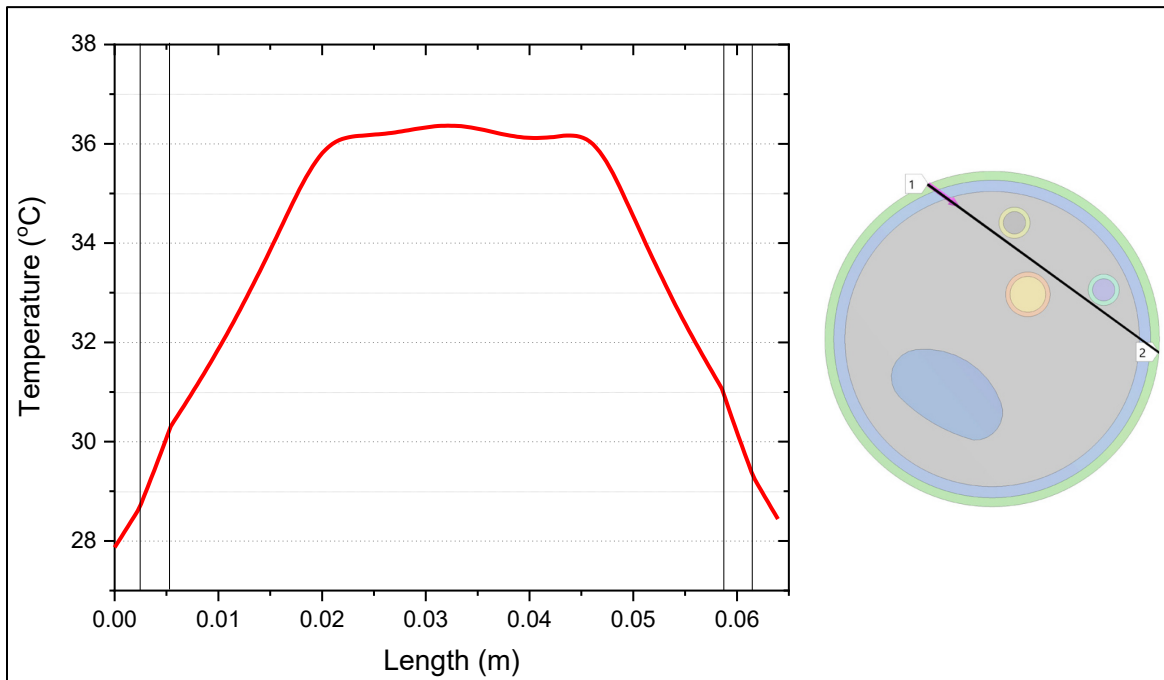


Figure 22: Temperature distribution along the path close to blood vessel in simplified human forearm

In Figure 21 it can be observed that heat flows from the blood vessels to the skin surface. Skin surface temperature near the top skin surface is higher because of the proximity of blood vessels in the region. As the geometry is uniform across the central axis, the temperature distribution is also consistent along this axis. The results from Figure 22 further confirm that the fat layer, indeed has the sharpest temperature drop across its length. The average skin surface temperature of about 27 °C was observed with an average model temperature of 31.5 °C. Furthermore, as the proportion of muscle is lower when compared to the cubic model, there is no observable rise in temperature above 37 °C.

5.1.3 Human forearm

This model provides a good starting point for testing the implementation on complex geometries. The stationary simulations are performed for different ambient temperatures from 5 °C to 35 °C and associated results are presented in Figure 28. Figure 23 - Figure 25 present the results at ambient temperature of 15 °C. In Figure 26 and Figure 27, the model results are compared with original measurements from Pennes' 1948 study [7].

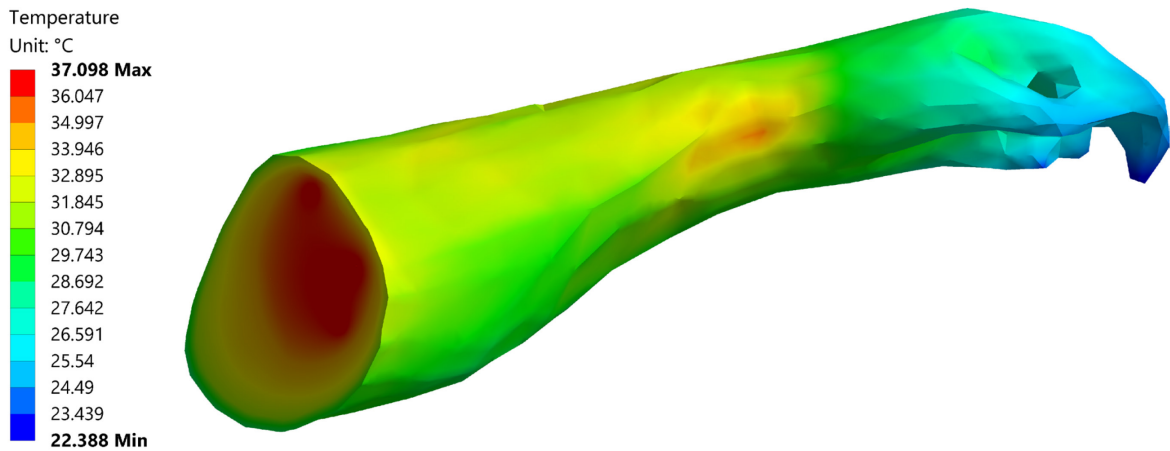


Figure 23: Contour plot of temperature distribution on realistic human forearm

The above image is an excellent depiction of the temperature distribution across the human forearm. The hand region, especially the fingers show a low temperature as a response to the low ambient temperature of 15 °C. An interesting observation from the figure is the wrist region, which shows a higher temperature (hot spot) close to the skin. This is attributed to the fact that the blood vessels are very close to the skin surface. The results also corroborate previously obtained results from the simplified geometry of the forearm, where the heat is transferred from the blood vessels to the surrounding tissue. It should also be noted that the resolution of the obtained results is limited owing to the low quality of the geometry.

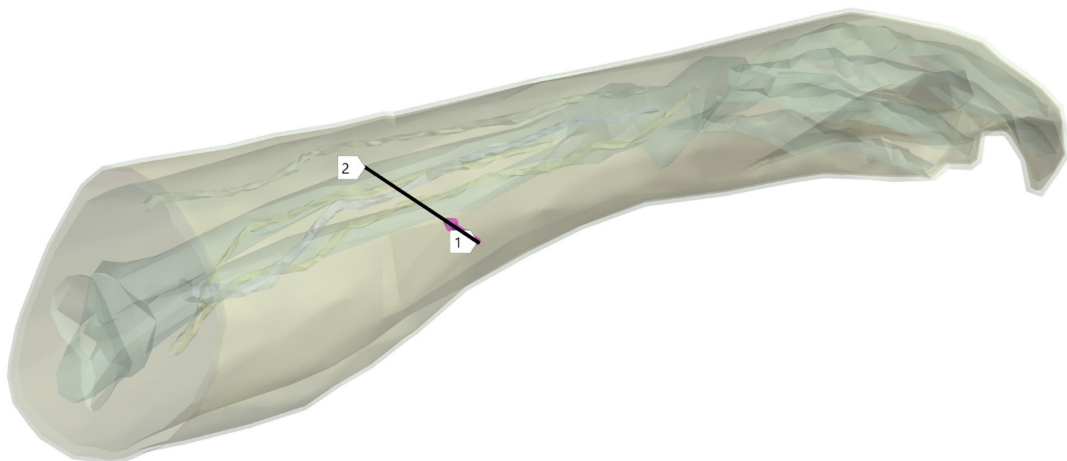


Figure 24: Path inside the human forearm

Figure 25 provides the temperature distribution along the path shown in Figure 24, the trend matches that of previous models, with the temperature drop across the fat layer. This reaffirms the validity of the implementation. As the path is not crossing any artery or vein the temperature does not rise above 37 °C.

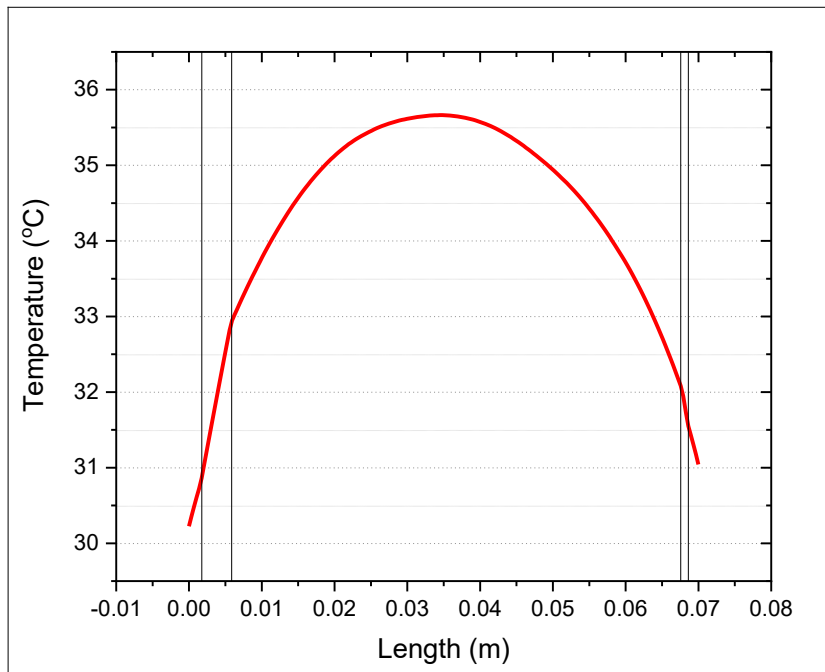


Figure 25: Temperature profile along path (Figure 24) in realistic human forearm at 15 °C

Figure 26 compares the internal temperature distribution in the forearm based on the measurements taken by Pennes for three subjects at an ambient temperature of 26.6 °C. It is observable that, the results closely follow the same trend as that of the measured values. The minor difference in the temperature values may be because of different locations of data measurement and variation in the forearm anatomy of the subjects as compared to modelled geometry.

In Figure 27, the surface temperatures along the long axis are shown at 25 °C room temperature. One thing to note is that the values were measured on the right forearm, whereas current analysis is done on the left forearm. The computed values in the middle of the forearm show a higher temperature than the measured values due to the proximity of blood vessel to the surface. The measured value at the top surface of hand is considerably greater than the computed value as the blood vessels terminate before reaching the hand in the current model as apparent from Figure 15.

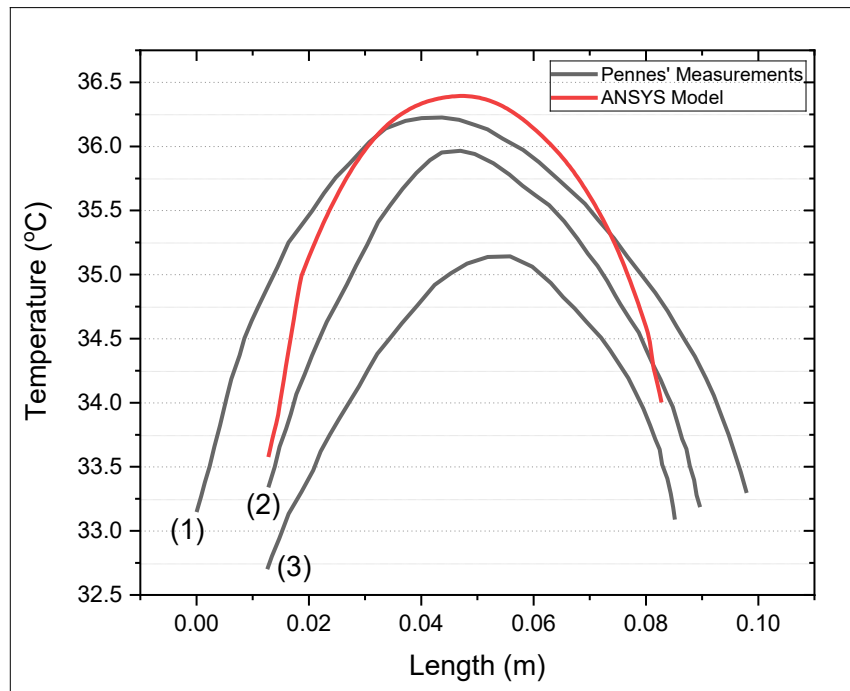


Figure 26: Comparison of ANSYS results with Pennes' measurements at 26.6 °C

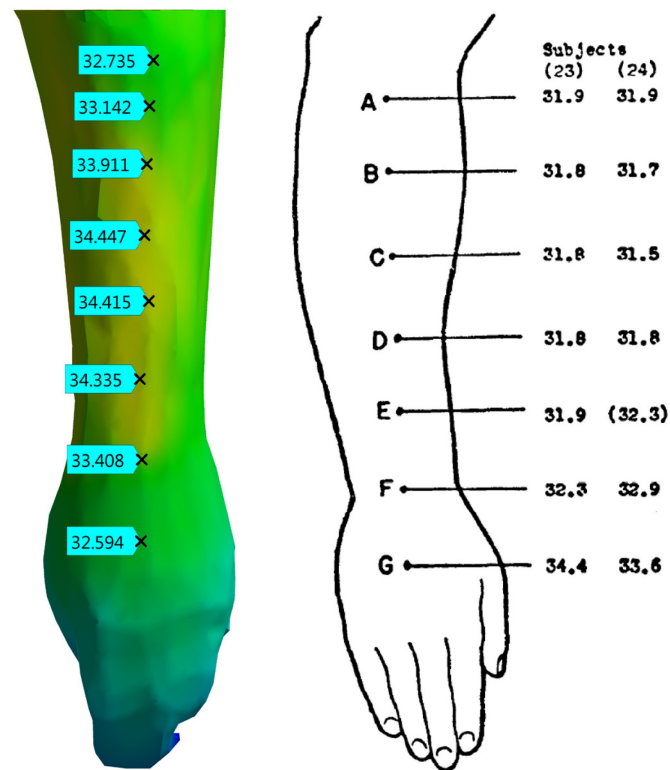


Figure 27: Temperature along long axis of arm at 25 °C compared to Pennes' measurements

From Figure 28 the temperature response of the model under various ambient temperatures can be seen. The maximum temperature does not rise over 37 °C even at a higher ambient temperature, whereas the skin surface and other average temperatures rise linearly with increase in ambient temperature. This could be due to adequate balance between the heat generated and heat liberated from the model without thermoregulation.

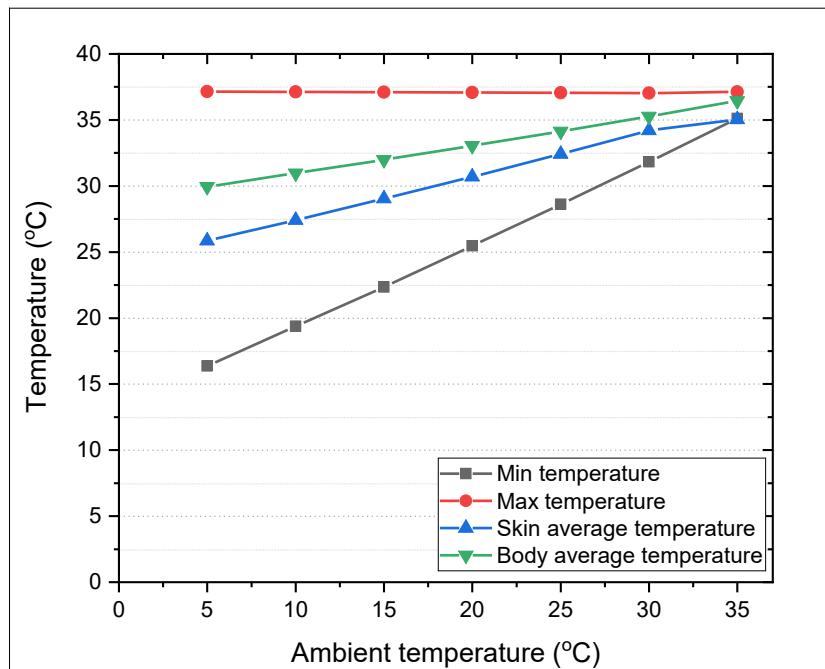


Figure 28: Various temperatures of the forearm in different environmental conditions

5.1.4 Torso

The human torso geometry is by far the most complex out of all the models, there are large number of different tissue geometries closely representing the human torso. The simulation for this model is done at 15 °C and the simulation was computed in 9 minutes and 40 seconds.

Figure 29 - Figure 33 detail the temperature distribution obtained in contour plots of skin surface and internal sections. Figure 34 shows the temperature distribution of the internal tissues. Furthermore, temperature profiles along different paths based on Figure 33 are also presented in Figure 35.

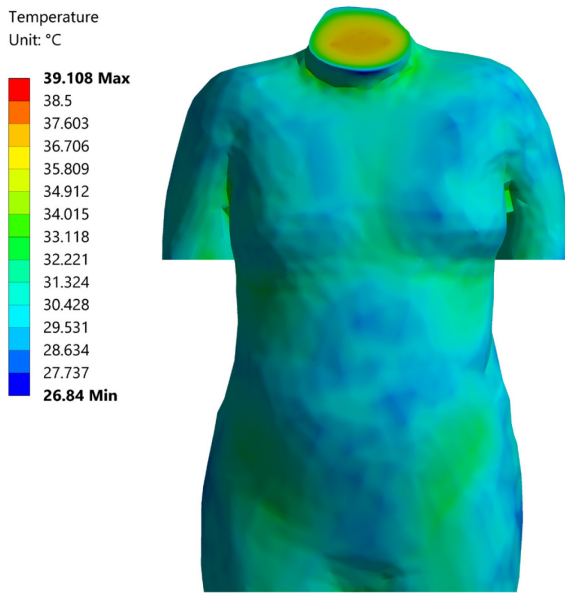


Figure 29: Torso, front view

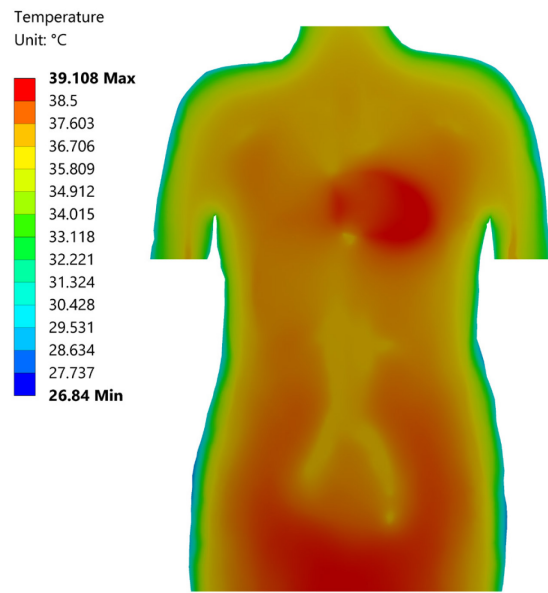


Figure 30: Torso, front view - section

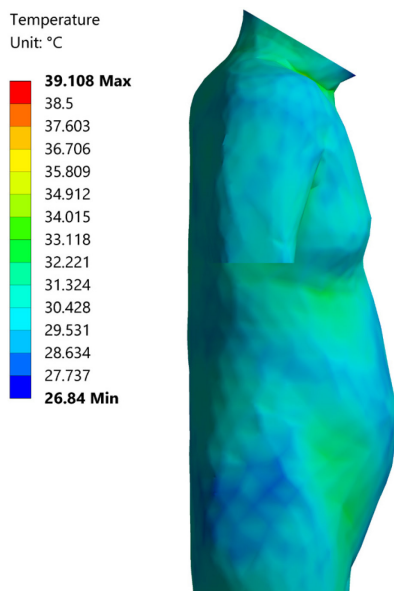


Figure 31: Torso, side view

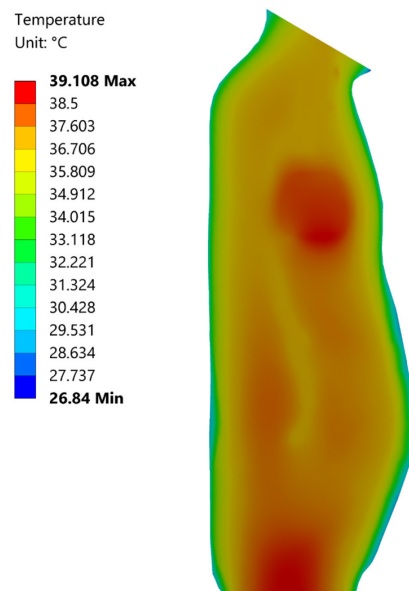


Figure 32: Torso, side view - section

Figure 29 - Figure 32 illustrate the temperature distribution across the skin surface and the temperature distribution on the section plane with the maximum temperature in the heart muscle. It can be observed that the regions of high fat concentration, such as the abdomen and lower periphery exhibit low skin surface temperature as compared to regions with low fat content. The area around the neck is also at significantly high temperature due to close

proximity of arteries and veins. Also, visible is the unusually high temperature ($>37^{\circ}\text{C}$) of certain regions in the chest and the abdomen. This was unavoidable due to the completely solid and highly faceted organ geometries. Physiologically, these organs are mostly thin walled structures filled with fluids such as blood, water or air depending on the organ. The apparent lack of insufficient cooling of the chest through respiration also contributed to the higher than normal temperature. Another possible explanation for unexpected temperatures in the abdomen can be attributed to the low quality of mesh, mainly due to large number of irregular geometries in this region along with the large volume of muscle. Despite this, the presence of these high temperatures in the heart muscle and near the rectum due to the high metabolic heat production and the subsequent temperature distribution obtained is nearly physiological.

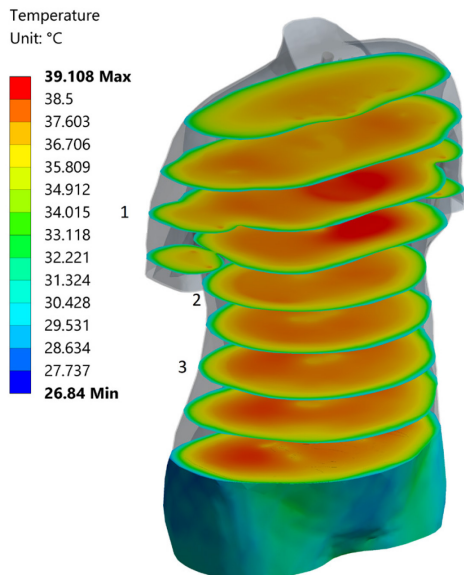


Figure 33: Torso, cross-sectional distribution

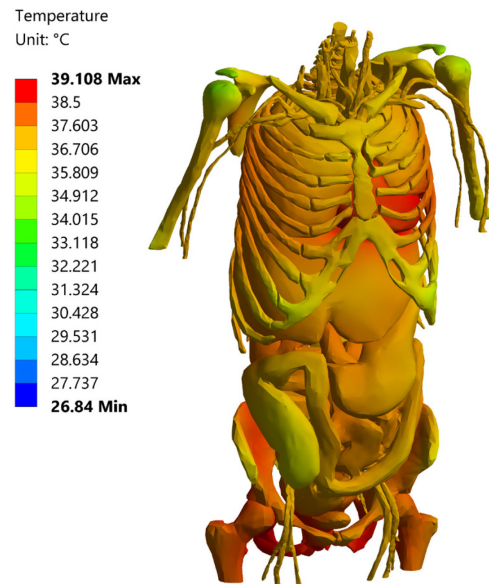


Figure 34: Torso, internal distribution

Figure 34 remarkably highlights the inhomogeneity of spatial distribution in the geometry across various cross section. Also observable from Figure 34 is the temperature distribution of the internal structure of the model, it can be seen that the temperature near the shoulder region is considerably lower because of the distance from blood vessels.

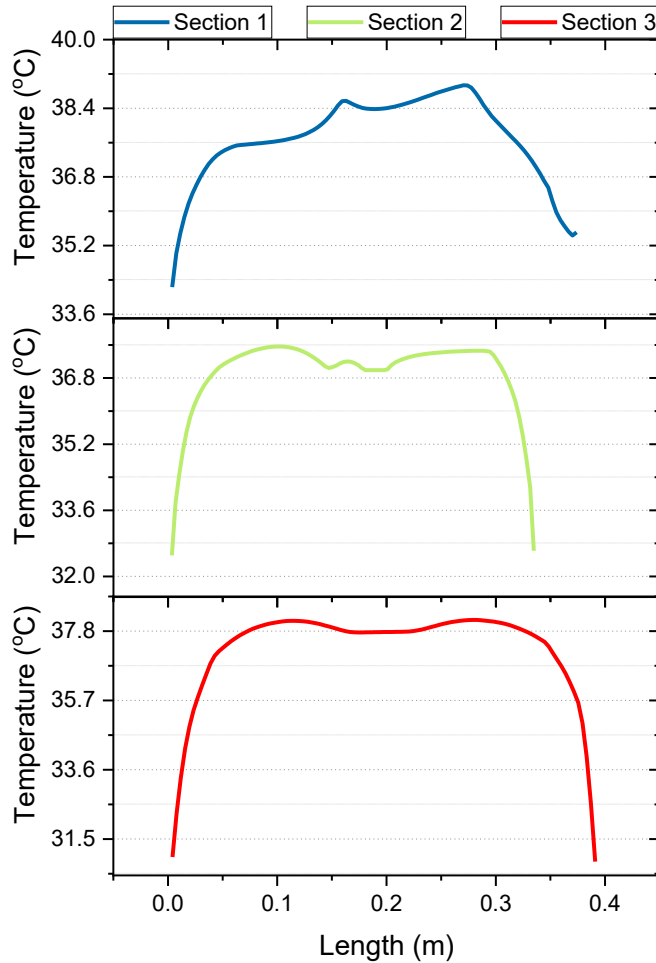


Figure 35: Temperature profiles along 3 sections from Figure 33

The above figure depicts the temperature profiles along different paths. In section 1 the regions between the two peaks is the heart muscle. Section 2 follows the path across the liver and part of the stomach, whereas the two peaks in section 3 are that of the left and right kidneys along the path. Despite a slight disagreement of the results with physiologically correct core temperatures, the findings of this study are in good accordance with respect to the trend of temperature distribution.

5.2 Thermoregulation in simplified cubic model

In this section, the results from the control loop simulations on the simplified cubic model are presented. Two sets of simulations are performed for an end time of 3,000 seconds, the first at an ambient temperature of 15 °C, to simulate a cold environment and the second at 25 °C for warm environment. The temperature distributions are presented in Figure 36 and Figure 37.

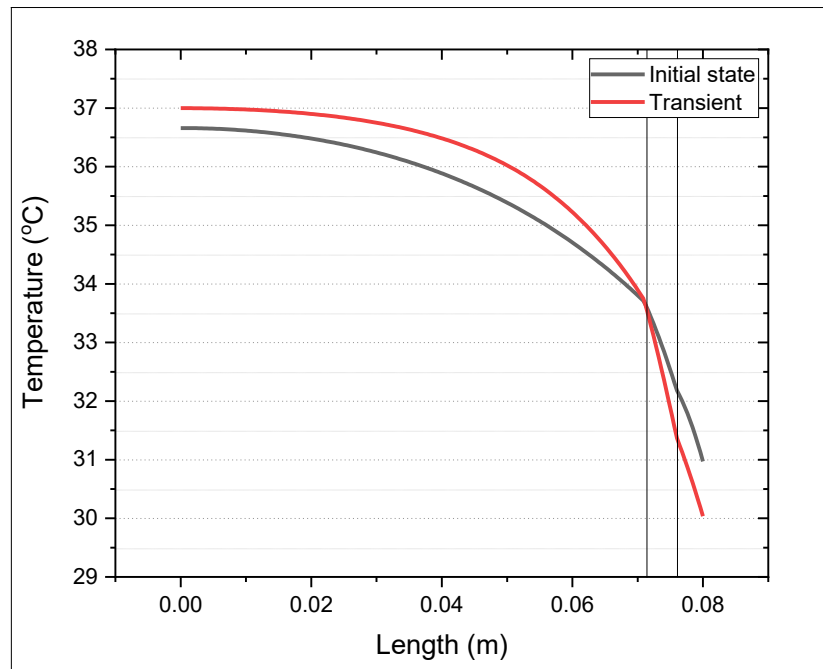


Figure 36: Temperature distribution of initial state and after control at 15 °C

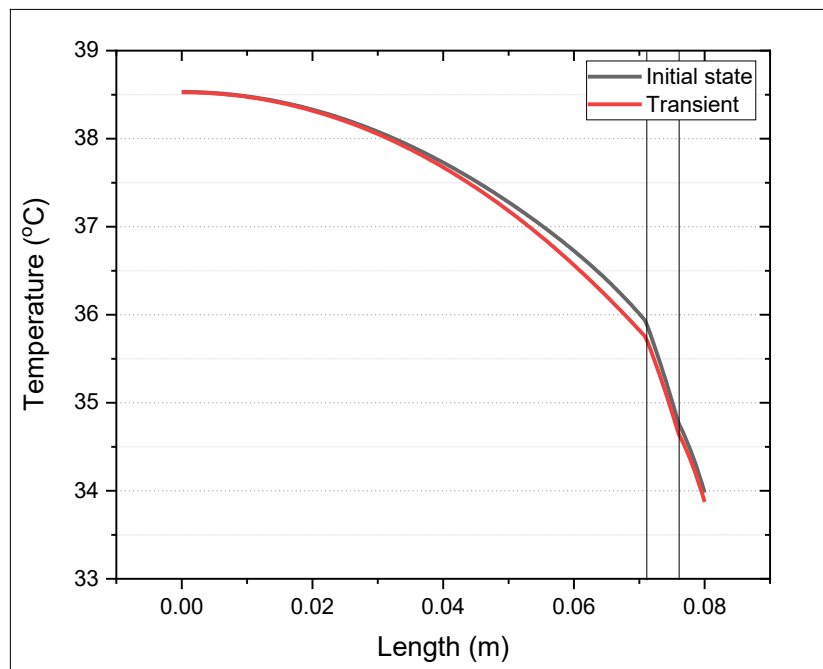


Figure 37: Temperature distribution of initial state and after control at 25 °C

Ambient temperature of 15 °C

From Figure 36, the core temperature of 36.6 °C is raised to 37 °C and skin temperature falls from 31 °C to 30.4 °C due to the controller action. Temperature of the muscle surface shows that there is a steady rise in temperature over time as a result of controller action, whereas the skin temperature drops due to constriction. As the ambient temperature is low, the skin wettedness factor remains constant at 0.06. The respective skin and muscle temperatures over time are available in Appendix 8.4, Figure 41 .

Ambient temperature of 25 °C

In response to warm environment, the skin blood flow is increased to allow for more heat to be dissipated from the skin. The temperature distribution from the Figure 37, shows that the skin temperature changes from 34 °C to 33.87. °C. However due to suspected low heat transfer from muscle and relatively high minimum blood perfusion rate, the muscle temperature remains relatively unchanged. It is also established from the stationary results in section 5.1.1, that the large muscle volume affects the amount of heat generated due to blood perfusion. In Appendix 8.4, Figure 42, muscle and skin temperature over time is presented.

6 Conclusion and Outlook

Numerous thermophysiological analyses have been conducted to study responses of the human thermal system. Both active and passive systems are analyzed for different boundary conditions. The idea of this project was to use a complex simulation model of the human body as a tool for evaluating temperature distribution due to various physiological processes. Various heat transfer mechanisms such as radiation, convection, evaporative heat flux, sweating, blood perfusion and metabolic heat generation are modelled. Each model provides useful insight into the understanding of the human thermal system.

The first set of analysis is carried out on simplified geometries. The simplified cubic tissue highlights the insulating effects of the fat layer. As the fat layer lies between the skin surface and the core, it has a direct effect on the overall heat transfer with the environment. A temperature drop of 1.6 K is observed across the fat layer. This trend of temperature change in the fat layer is further confirmed by the temperature profiles from other models as well. As a consequence of large muscle thickness, the core temperature rises above 37 °C due to high heat generation from bioheat equation.

The simplified human forearm incorporates a concentric tissue structure with off-center blood vessels and bone. The blood vessels act as a source of heat and the skin surface transfers the heat to the environment. The muscle volume is considerably lower as compared to the cubic model, thus the muscle temperature does not rise above 36.7 °C. It can be concluded that the volume and the proportion of the muscle has a large effect on the core temperature for the current implementation of bioheat equation.

Furthermore, simulations are performed for the realistic human geometries. The results from the forearm model are compared against the original measurements from Penne's 1948 research [7] at 26.6 °C ambient temperature. The results confirm that the simulations are in good agreement with the measurements. The model is further simulated for different ambient temperatures. It is important to note that the core temperature does not rise above 37 °C, while the skin temperature along with overall average temperature rises.

The thermal simulation of the torso model presents the limitations of the geometry that is being used. The available metabolic heat generation rates are adjusted to the solid volume

of the internal organs such as the heart, lungs, stomach etc. The results also show the restrictive resolution of different tissues in the model. However, regardless of these limitations, the temperature distribution obtained is noteworthy of the trends observed in previous models. The results demonstrate that for current application, consideration of inhomogeneity in the human body is of great importance. The temperature distributions across various sections highlight favorable locations for the TEG-powered implants. From Figure 29 - Figure 33, the chest along with lower left and lower right regions of the abdomen exhibit reasonably high temperature gradients across varying thickness of the fat layer. For low profile implants, locations with moderate temperature drops like the upper shoulder region could also prove to be sufficient for fulfilling the power needs of the implant. A high temperature gradient is observable in the abdomen, though it should be noted that because of its remoteness, this area might not be suitable for deep brain stimulation and other upper body implants. Sourcing a human body geometry with better resolution especially for various internal organs and cardiovascular system would allow for an improved physiologically accurate analysis.

Finally, active system was simulated for two separate ambient temperatures. The control system performs reasonably well in response to cold environment. However from the results, the limitations of the control loop for warm environments are apparent due to the limitation of blood perfusion rates based on the minimum and maximum values from database. It is safe to assume that the manner in which the control loop has been implemented still has room for improvement. Despite this, this work could prove to be a starting point for implementation of more complex thermoregulatory mechanisms such as shivering, respiratory losses etc.

Although the models here are simulated for calculating the temperature distributions for optimal TEG operation, long term applications could be to expand the model further to include thermal comfort effects for evaluating the thermal responses of the body in enclosed environments such as buildings, transportation etc. and study localized cooling strategies for hypothermic treatments.

Future work could take into account the aspects of the implant itself complete with the TEG, battery and supporting electronics in a hermetically sealed housing to analyze the behavior of the implant under physiological conditions.

7 References

- [1] A. Chen, "Thermal Energy Harvesting with Thermoelectrics for Self-powered Sensors: With Applications to Implantable Medical Devices, Body Sensor Networks and Aging in Place," PhD, University of California, Berkeley, 2011.
- [2] Parsonnet, V. and Cheema, A., "The Nature and Frequency of Postimplant Surgical Interventions," *Pacing and Clinical Electrophysiology*, no. 26(12), pp.2308-2312., 2003.
- [3] A. Ben Amar, A. B. Kouki, and H. Cao, "Power Approaches for Implantable Medical Devices," (eng), *Sensors (Basel, Switzerland)*, vol. 15, no. 11, pp. 28889–28914, 2015.
- [4] M. Rasouli and L. S. J. Phee, "Energy sources and their development for application in medical devices," (eng), *Expert review of medical devices*, vol. 7, no. 5, pp. 693–709, 2010.
- [5] K. Parsons, *Human thermal environments*, 3rd ed.: CRC Press, Taylor & Francis, 2014.
- [6] Y. Yang, X.-J. Wei, and J. Liu, "Suitability of a thermoelectric power generator for implantable medical electronic devices," *J. Phys. D: Appl. Phys.*, vol. 40, no. 18, pp. 5790–5800, 2007.
- [7] H. H. Pennes, "Analysis of Tissue and Arterial Blood Temperatures in the Resting Human Forearm," *Journal of applied physiology (Bethesda, Md. : 1985)*, vol. 1, no. 2, pp. 93–122, 1948.
- [8] M. M. Chen and K. R. Holmes, "Microvascular contributions in tissue heat transfer," *Ann NY Acad Sci*, vol. 335, no. 1 Thermal Chara, pp. 137–150, 1980.
- [9] W. J. Song, S. Weinbaum, L. M. Jiji, and D. Lemons, "A Combined Macro and Microvascular Model for Whole Limb Heat Transfer," *J. Biomech. Eng.*, vol. 110, no. 4, p. 259, 1988.
- [10] S. Weinbaum, L. Jiji, and D. E. Lemons, "Theory and experiment for the effect of vascular temperature on surface tissue heat transfer—Part 1: anatomical foundation and model conceptualization," *ASME J. Biomech. Eng.*, vol. 106, pp. 246–251, 1984.
- [11] E. H. Wissler, "Pennes' 1948 paper revisited," *Journal of applied physiology (Bethesda, Md. : 1985)*, vol. 85, no. 1, pp. 35–41, 1998.
- [12] P. A. Gagge, J. J. A. Stolwijk, and Y. Nishi, "An Effective Temperature Scale Based on a Simple Model of Human Physiological Regulatiry Response," *ASHRAE Transactions*, vol. 77, pp. 247–262, 1971.

- [13] P. A. Gagge, A. P. Fobelets, and L. G. Berglund, "A standard predictive index of human response to the thermal environment," *ASHRAE Transactions*, vol. 92 (2b), pp. 709–731, 1986.
- [14] J. A. J. Stolwijk, "A mathematical model of physiological temperature regulation in man," NASA, Washington DC, NASA contractor report, 1971.
- [15] J. J. A. Stolwijk and J. D. Hardy, "Control of Body Temperature," *Handbook of Physiology, American Physiological Society.*, 1977.
- [16] R. G. Gordon, R. B. Roemer, and S. M. Horvath, "A Mathematical Model of the Human Temperature Regulatory System - Transient Cold Exposure Response," *IEEE Trans. Biomed. Eng.*, vol. BME-23, no. 6, pp. 434–444, 1976.
- [17] E. H. Wissler, "A mathematical model of the human thermal system," *Bulletin of mathematical biophysics*, vol. 26, pp. 147–166, 1964.
- [18] E. H. Wissler, "Mathematical simulation of human thermal behavior using whole body models," *Heat transfer in medicine and biology*, vol. 1, no. 13, pp. 325–373, 1985.
- [19] D. Fiala, "Dynamic Simulation of Human Heat Transfer and Thermal Comfort," PhD, Institute of Energy and Sustainable Development, De Montfort University, 1998.
- [20] D. Fiala, K. J. Lomas, and M. Stohrer, "A computer model of human thermoregulation for a wide range of environmental conditions: the passive system," (eng), *Journal of applied physiology (Bethesda, Md. : 1985)*, vol. 87, no. 5, pp. 1957–1972, 1999.
- [21] D. Fiala, K. J. Lomas, and M. Stohrer, "Computer prediction of human thermoregulatory and temperature responses to a wide range of environmental conditions," *International journal of biometeorology*, vol. 45, no. 3, pp. 143–159, 2001.
- [22] C. E. Smith, "A Transient, Three-dimensional Model of the Human Thermal System," PhD, Kansas State University, 1991.
- [23] M. Salloum, N. Ghaddar, and K. Ghali, "A new transient bioheat model of the human body and its integration to clothing models," *International Journal of Thermal Sciences*, vol. 46, no. 4, pp. 371–384, 2007.
- [24] J. Werner and M. Buse, "Temperature profiles with respect to inhomogeneity and geometry of human body," 1988.
- [25] A. C. Guyton and J. E. Hall, *Textbook of Medical Physiology*, 11th ed.: Elsevier Saunders, 2006.
- [26] A. Despopoulos and S. Silbernagl, *Color Atlas of Physiology*, 5th ed.: Thieme, 2002.

- [27] S. Murakami, S. Kato, and J. Zeng, "Combined simulation of airflow, radiation and moisture transport for heat release from a human body," *Building and Environment*, vol. 35, no. 6, pp. 489–500, 2000.
- [28] D. Mitchell, "Convective heat transfer in man and other animals," *Heat loss from animals and man: assessment and control*, 1974.
- [29] J. D. Hardy and E. F. DuBois, "Regulation of Heat Loss from the Human Body," (eng), *Proceedings of the National Academy of Sciences*, vol. 23, no. 12, pp. 624–631, 1937.
- [30] OpenStax CNX, *OpenStax, Anatomy & Physiology*. [Online] Available: <http://cnx.org/contents/14fb4ad7-39a1-4eee-ab6e-3ef2482e3e22@6.27>.
- [31] D. M. Rowe, *CRC handbook of thermoelectrics*. Boca Raton, Fl., London: CRC Press, 1995.
- [32] M. Strasser, R. Aigner, M. Franosch, and G. Wachutka, "Miniaturized thermoelectric generators based on poly-Si and poly-SiGe surface micromachining," *Sensors and Actuators A: Physical*, vol. 97-98, pp. 535–542, 2002.
- [33] T. M. Tritt, "Thermoelectric Materials: Principles, Structure, Properties, and Applications," in *Encyclopedia of Materials: Science and Technology*: Elsevier, 2002.
- [34] P. A. Hasgall *et al.*, "IT'IS Database for thermal and electromagnetic parameters of biological tissues," [Online] Available: www.itis.ethz.ch/database.
- [35] ANSYS® Academic Research Mechanical, *Release 19.0, Help System, Mechanical APDL*: ANSYS, Inc.
- [36] S. Makarov, G. Noetscher, and J. Yanamadala, *VHP-Female Datasets*.
- [37] S. N. Makarov *et al.*, "Virtual Human Models for Electromagnetic Studies and Their Applications," *IEEE Rev. Biomed. Eng.*, vol. 10, pp. 95–121, 2017.
- [38] J. Yanamadala *et al.*, "Multi-purpose VHP-female version 3.0 cross-platform computational human model," in *2016 10th European Conference on Antennas and Propagation (EuCAP)*, Davos, Switzerland, 2016, pp. 1–5.
- [39] U.S. National Library of Medicine, "*The Visible Human Project®*". Available: https://www.nlm.nih.gov/research/visible/visible_human.html.
- [40] F. E. M. Janssen, G. M. J. van Leeuwen, and A. A. van Steenhoven, "Numerical Simulation of Scalp Cooling to Prevent Chemotherapy-Induced Alopecia,"

8 Appendix

8.1 APDL commands

Table 8: APDL command for evaporative heat loss

```

!Evaporative loss

hc = ARG5      ! convection coefficient (3.1)
ta = ARG6      ! ambient Temperature (15)
phi = ARG7     ! relative humidity (0.5)
w = ARG8       ! skin wettedness (0.06)

*DIM,evap,TABLE,35,1,1,TEMP,
!TEMP values

evap(1,0,1) = 20
evap(2,0,1) = 20.5
evap(3,0,1) = 21
evap(4,0,1) = 21.5
evap(5,0,1) = 22
evap(6,0,1) = 22.5
evap(7,0,1) = 23
evap(8,0,1) = 23.5
evap(9,0,1) = 24
evap(10,0,1) = 24.5
evap(11,0,1) = 25
evap(12,0,1) = 25.5
evap(13,0,1) = 26
evap(14,0,1) = 26.5
evap(15,0,1) = 27
evap(16,0,1) = 27.5
evap(17,0,1) = 28
evap(18,0,1) = 28.5
evap(19,0,1) = 29
evap(20,0,1) = 29.5
evap(21,0,1) = 30
evap(22,0,1) = 30.5
evap(23,0,1) = 31
evap(24,0,1) = 31.5
evap(25,0,1) = 32
evap(26,0,1) = 32.5
evap(27,0,1) = 33
evap(28,0,1) = 33.5
evap(29,0,1) = 34
evap(30,0,1) = 34.5
evap(31,0,1) = 35
evap(32,0,1) = 35.5
evap(33,0,1) = 36
evap(34,0,1) = 36.5
evap(35,0,1) = 37

!evap HFLUX

evap(1,1,1) = -(16.5*w*hc*0.1*((exp(18.956-(4030.18/(20+235))))-(phi*(exp(18.956-
(4030.18/(ta+235)))))))
evap(2,1,1) = -(16.5*w*hc*0.1*((exp(18.956-(4030.18/(20.5+235))))-(phi*(exp(18.956-
(4030.18/(ta+235)))))))
evap(3,1,1) = -(16.5*w*hc*0.1*((exp(18.956-(4030.18/(21+235))))-(phi*(exp(18.956-
(4030.18/(ta+235)))))))
evap(4,1,1) = -(16.5*w*hc*0.1*((exp(18.956-(4030.18/(21.5+235))))-(phi*(exp(18.956-
(4030.18/(ta+235)))))))
evap(5,1,1) = -(16.5*w*hc*0.1*((exp(18.956-(4030.18/(22+235))))-(phi*(exp(18.956-
(4030.18/(ta+235)))))))
evap(6,1,1) = -(16.5*w*hc*0.1*((exp(18.956-(4030.18/(22.5+235))))-(phi*(exp(18.956-
(4030.18/(ta+235)))))))

```


Table 9: APDL command for heat generation for tissue

```

rho = 1049.75 ! kg 1/m^3
c = 3617      ! J 1/kg 1/K

! Perfusion in Muscle
omega_muscle = 0.000337      ! 1/s
Q_muscle = 498.5245          ! W/m^3
*DIM,perfusionmuscle,TABLE,2,1,1,TEMP,
! TEMP values
perfusionmuscle(1,0,1) = 15
perfusionmuscle(2,0,1) = 37

! HGEN values
perfusionmuscle(1,1,1) = (rho*c*omega_muscle*(37-15) + Q_muscle)
perfusionmuscle(2,1,1) = (rho*c*omega_muscle*0. + Q_muscle)

! Perfusion in Fat
omega_fat = 0.000301116     ! 1/s
Q_fat = 279.8009561          ! W/m^3
*DIM,perfusionfat,TABLE,2,1,1,TEMP,
! TEMP values
perfusionfat(1,0,1) = 15
perfusionfat(2,0,1) = 37

! HGEN values
perfusionfat(1,1,1) = (rho*c*omega_fat*(37-15) + Q_fat)
perfusionfat(2,1,1) = (rho*c*omega_fat*0. + Q_fat)

! Perfusion in skin
omega_skin = 0.000905683    ! 1/s
Q_skin = 841.5732636         ! W/m^3
*DIM,perfusionskin,TABLE,2,1,1,TEMP,
! TEMP values
perfusionskin(1,0,1) = 15
perfusionskin(2,0,1) = 37

! HGEN values
perfusionskin(1,1,1) = (rho*c*omega_skin*(37-15) + Q_skin)
perfusionskin(2,1,1) = (rho*c*omega_skin*0. + Q_skin)

cmsel,s,muscle
bfe,all,hgen,,%perfusionmuscle%
cmsel,s,fat
bfe,all,hgen,,%perfusionfat%
cmsel,s,skin
bfe,all,hgen,,%perfusionskin%
ALLSEL

```

Table 10: APDL command for control in active system

```

!Sweating
hc = ARG5      !film coeff. (3.1)
ta = ARG6      ! ambient Temperature (15)
phi = ARG7     ! humidity (0.5)
w = ARG8       ! sweating efficency (0.132)
rho = 1049.75 ! kg 1/m^3
c = 3617      ! J 1/kg 1/K
! Perfusion in Fat
omega_fat = 0.000301116 ! 1/s
Q_fat = 279.8009561      ! W/m^3
*DIM,perfusionfat,TABLE,2,1,1,TEMP,
! TEMP values
perfusionfat(1,0,1) = 0.
perfusionfat(2,0,1) = 37
! HGEN values
perfusionfat(1,1,1) = rho*c*omega_fat*37 + Q_fat

```

```

perfusionfat(2,1,1) = rho*c*omega_fat*0. + Q_fat
controller=3
*DIM,TempNode,CHAR,controller,1,1, , ,
TempNode(1,1,1) ='muscle_s'
TempNode(2,1,1) ='skin_s'
TempNode(3,1,1) ='skin_s'
*DIM,Tempavg,ARRAY,controller,1,1, ,
*DIM,Kp_AR,ARRAY,controller,1,1, ,
Kp_AR(1,1,1) =ARG1
Kp_AR(2,1,1) =ARG2
Kp_AR(3,1,1) =ARG9
*DIM,err,ARRAY,controller,1,1, ,
*DIM,fact,ARRAY,controller,1,1, ,
dt=15
ts=3001
*DO,t,1,ts,dt
J=1
    /NOPR
    *GET,CurLS,ACTIVE,0,SET,LSTP
    *IF,CurLS,EQ,0,THEN
        fini
        /config,noeldb,0
        /solu
    *ENDIF
    cmsel,s,%TempNode(J,1,1)%
    *GET,NumNods,NODE,0,COUNT
    *GET,minnods,NODE,,NUM,MIN
    cnn=minnods
    Tempsum=0.0
    *GET,maxnods,NODE,,NUM,MAX
    lasy=(minnods+NumNods)
    *DO,I,minnods,lasy,1
        cnn=NDNEXT(cnn)
        val=0
        *GET,val,NODE,cnn,TEMP,
        Tempsum = Tempsum + val
    *ENDDO
    /GOPR
    Tempavg(J,1,1)= Tempsum/NumNods
    omega_muscle = 0.000337 ! 1/s
    Q_muscle = 498.5245 ! W/m^3
    *DIM,perfusionmuscle,TABLE,2,1,1,TEMP,
    ! TEMP values
    perfusionmuscle(1,0,1) = 0.
    perfusionmuscle(2,0,1) = 37
    Td = ARG3
    err(J,1,1)=Td-Tempavg(J,1,1)
    fact(J,1,1)=(Kp_AR(J,1,1)*(err(J,1,1)))
    omega_muscle_n=omega_muscle*fact(J,1,1)
    *IF,omega_muscle_n,LT,0,THEN
        omega_muscle_n=0
        perfusionmuscle(1,1,1) = rho*c*omega_muscle_n*37 + Q_muscle
        perfusionmuscle(2,1,1) = rho*c*omega_muscle_n*0 + Q_muscle
        cmsel,s,muscle
        bfe,all,hgen,,%perfusionmuscle%
        ALLS
    *ELSEIF,omega_muscle_n,GT,0,AND,omega_muscle_n,LT,0.000336873,THEN
        omega_muscle_n=0.000336873
        perfusionmuscle(1,1,1) = rho*c*omega_muscle_n*37 + Q_muscle
        perfusionmuscle(2,1,1) = rho*c*omega_muscle_n*0 + Q_muscle
        cmsel,s,muscle
        bfe,all,hgen,,%perfusionmuscle%
        ALLS
    *ELSEIF,omega_muscle_n,GT,0.000336873,AND,omega_muscle_n,LT,0.001712776,THEN
        perfusionmuscle(1,1,1) = rho*c*omega_muscle_n*37 + Q_muscle
        perfusionmuscle(2,1,1) = rho*c*omega_muscle_n*0 + Q_muscle
        cmsel,s,muscle
        bfe,all,hgen,,%perfusionmuscle%
        ALLS
    *ELSEIF,omega_muscle_n,GT,0.001712776,THEN
        omega_muscle_n=0.001712776
        perfusionmuscle(1,1,1) = rho*c*omega_muscle_n*37 + Q_muscle

```

```

        perfusionmuscle(2,1,1) = rho*c*omega_muscle_n*0 + Q_muscle
        cmsel,s,muscle
        bfe,all,hgen,,%perfusionmuscle%
        ALLS
    *ENDIF
j=2
/NOPR
*GET,CurLS,ACTIVE,0,SET,LSTP
*IF,CurLS,EQ,0,THEN
    fini
    /config,noeldb,0
    /solu
*ENDIF
cmsel,s,%TempNode(J,1,1)%
*GET,NumNods,NODE,0,COUNT
*GET,minnods,NODE,,NUM,MIN
cnn=minnods
Tempsum=0.0
*GET,maxnods,NODE,,NUM,MAX
lasy=(minnods+NumNods)
*DO,I,minnods,lasy,1
    cnn=NDNEXT(cnn)
    val=0
    *GET,val,NODE,cnn,TEMP,
    Tempsum = Tempsum + val
*ENDDO
/GOPR
Tempavg(J,1,1)= Tempsum/NumNods
omega_skin = 0.000905683 ! 1/s
Q_skin = 841.5732636 ! W/m^3
alpha=0.1945
bf=0.0695
Td = ARG4
err(J,1,1)= Td-Tempavg(J,1,1)
fact(J,1,1)=(Kp_AR(J,1,1)*(err(J,1,1)))
omega_skin = omega_skin*(1/(1+(alpha*bf)))
*DIM,perfusionskin,TABLE,2,1,1,TEMP,
! TEMP values
perfusionskin(1,0,1) = 0.
perfusionskin(2,0,1) = 37
omega_skin_n=omega_skin*fact(J,1,1)
*IF,omega_skin_n,LT,0,THEN
    omega_skin_n=0
    perfusionskin(1,1,1) = rho*c*omega_skin_n*37 + Q_skin
    perfusionskin(2,1,1) = rho*c*omega_skin_n*0 + Q_skin
    cmsel,s,skin
    bfe,all,hgen,,%perfusionskin%
    ALLS
*ELSEIF,omega_skin_n,GT,0,AND,omega_muscle_n,LT,0.000905683,THEN
    omega_skin_n=0.000905683
    perfusionskin(1,1,1) = rho*c*omega_skin_n*37 + Q_skin
    perfusionskin(2,1,1) = rho*c*omega_skin_n*0 + Q_skin
    cmsel,s,skin
    bfe,all,hgen,,%perfusionskin%
    ALLS
*ELSEIF,omega_skin_n,GT,0.000905683,AND,omega_muscle_n,LT,0.003227302,THEN
    perfusionskin(1,1,1) = rho*c*omega_skin_n*37 + Q_skin
    perfusionskin(2,1,1) = rho*c*omega_skin_n*0 + Q_skin
    cmsel,s,skin
    bfe,all,hgen,,%perfusionskin%
    ALLS
*ELSEIF,omega_skin_n,GT,0.003227302,THEN
    omega_skin_n=0.003227302
    perfusionskin(1,1,1) = rho*c*omega_skin_n*37 + Q_skin
    perfusionskin(2,1,1) = rho*c*omega_skin_n*0 + Q_skin
    cmsel,s,skin
    bfe,all,hgen,,%perfusionskin%
    ALLS
*ENDIF
j=3
/NOPR
*GET,CurLS,ACTIVE,0,SET,LSTP

```

```

*IF,CurLS,EQ,0,THEN
    fini
    /config,noeldb,0
    /solu
*ENDIF
cmsel,s,%TempNode(J,1,1)%
*GET,NumNods,NODE,0,COUNT
*GET,minnods,NODE,,NUM,MIN
cnn=minnods
Tempsum=0.0
*GET,maxnods,NODE,,NUM,MAX
lasy=(minnods+NumNods)
*DO,I,minnods,lasy,1
    cnn=NDNEXT(cnn)
    val=0
    *GET,val,NODE,cnn,TEMP,
    Tempsum = Tempsum + val
*ENDDO
/GOPR
Tempavg(J,1,1)= Tempsum/NumNods
*DIM,sweating,TABLE,2,1,1,TEMP,
!TEMP values
sweating(1,0,1) = 20
sweating(2,0,1) = 37
Td = ARG4
err(J,1,1)= Td-Tempavg(J,1,1)
fact(J,1,1)=(Kp_AR(J,1,1)*(err(J,1,1)))
w_n=w*(-fact(J,1,1))
*IF,w_n,LT,0,THEN
    w_n=0.06
    sweating(1,1,1) = -(16.5*w_n*hc*0.1*((exp(18.956-
(4030.18/(20+235)))-(phi*(exp(18.956-(4030.18/(ta+235)))))))
    sweating(2,1,1) = -(16.5*w_n*hc*0.1*((exp(18.956-
(4030.18/(37+235)))-(phi*(exp(18.956-(4030.18/(ta+235)))))))
    cmsel,s,fat
    bfe,all,hgen,,%perfusionfat%
    cmsel,s,skin
    cmsel,s,skin_s
    sf,all,hflux,%sweating%
    ALLS
*ELSEIF,w_n,GT,1,THEN
    w_n=1
    sweating(1,1,1) = -(16.5*w_n*hc*0.1*((exp(18.956-
(4030.18/(20+235)))-(phi*(exp(18.956-(4030.18/(ta+235)))))))
    sweating(2,1,1) = -(16.5*w_n*hc*0.1*((exp(18.956-
(4030.18/(37+235)))-(phi*(exp(18.956-(4030.18/(ta+235)))))))
    cmsel,s,fat
    bfe,all,hgen,,%perfusionfat%
    cmsel,s,skin
    cmsel,s,skin_s
    sf,all,hflux,%sweating%
    ALLS
*ELSE
    sweating(1,1,1) = -(16.5*w_n*hc*0.1*((exp(18.956-
(4030.18/(20+235)))-(phi*(exp(18.956-(4030.18/(ta+235)))))))
    sweating(2,1,1) = -(16.5*w_n*hc*0.1*((exp(18.956-
(4030.18/(37+235)))-(phi*(exp(18.956-(4030.18/(ta+235)))))))
    cmsel,s,fat
    bfe,all,hgen,,%perfusionfat%
    cmsel,s,skin
    cmsel,s,skin_s
    sf,all,hflux,%sweating%
    ALLS
*ENDIF
time,t
solve
*ENDDO

```

Table 11: Heat generation load application for torso

```

cmsel,s,muscle
bfe,all,hgen,,%perfusionmuscle%

cmsel,s,fat
bfe,all,hgen,,%perfusionfat%

cmsel,s,skin
bfe,all,hgen,,%perfusionskin%

cmsel,s,skin_s
sf,all,hflux,%sweating%

cmsel,s,bone
bfe,all,hgen,,%perfusionbones%

cmsel,s,bladder_s
bf,all,hgen,%perfusionbladder%

cmsel,s,heart_s
bf,all,hgen,%perfusionheart%

cmsel,s,intestine_s
bf,all,hgen,%perfusionintestine%

cmsel,s,kidney_s
bf,all,hgen,%perfusionkidney%

cmsel,s,liver_s
bf,all,hgen,%perfusionliver%

cmsel,s,lungs_s
bf,all,hgen,%perfusionlungs%

cmsel,s,stomach_s
bf,all,hgen,%perfusionstomach%

cmsel,s,trachea_s
bf,all,hgen,%perfusiontrachea%

cmsel,s,uterus_s
bf,all,hgen,%perfusionuterus%

```

8.2 Analysis settings

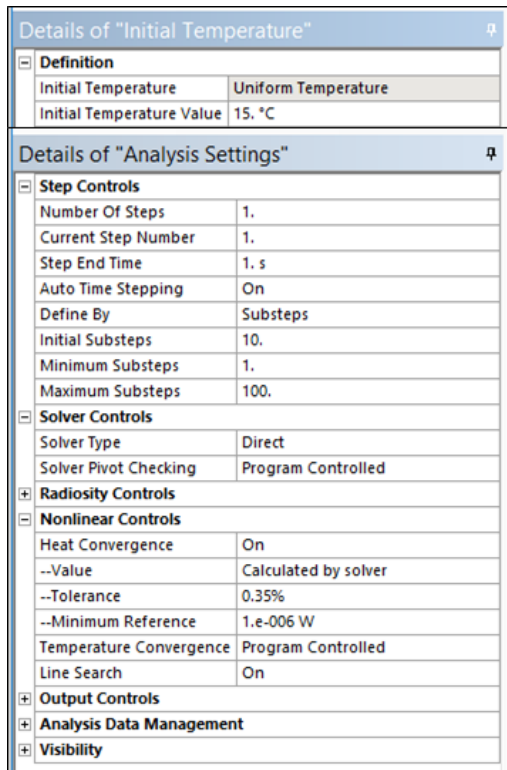


Figure 38: Analysis settings for stationary simulations

8.3 Torso model details

Table 12: Adjusted metabolic heat generation rates for torso model

Tissue	Thin-wall to solid Factor (-)	Heat Generation Rate (W/m ³)
Heart Muscle	0.322264	8157.06618
Kidney	0.049691	656.9845823
Large Intestine	0.317718	1793.410966
Liver	0.153105	804.4162387
Lung	0.36267	157.7316869
Stomach	0.179017	319.1022364
Trachea	0.184018	107.7249966
Urinary Bladder Wall	0.457352	599.9834208
Uterus	0.463042	1346.478043

8.4 Supplementary results

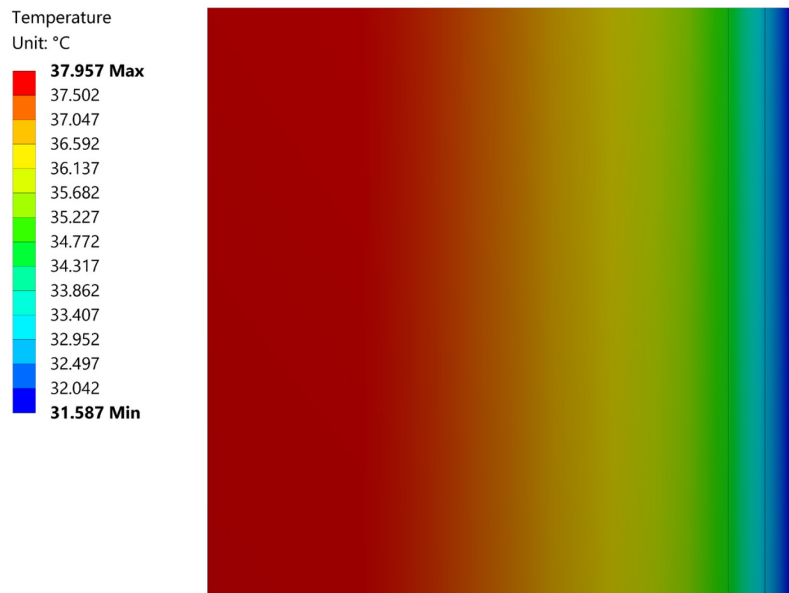


Figure 39: Temperature contour of simplified cubic geometry at 15 °C

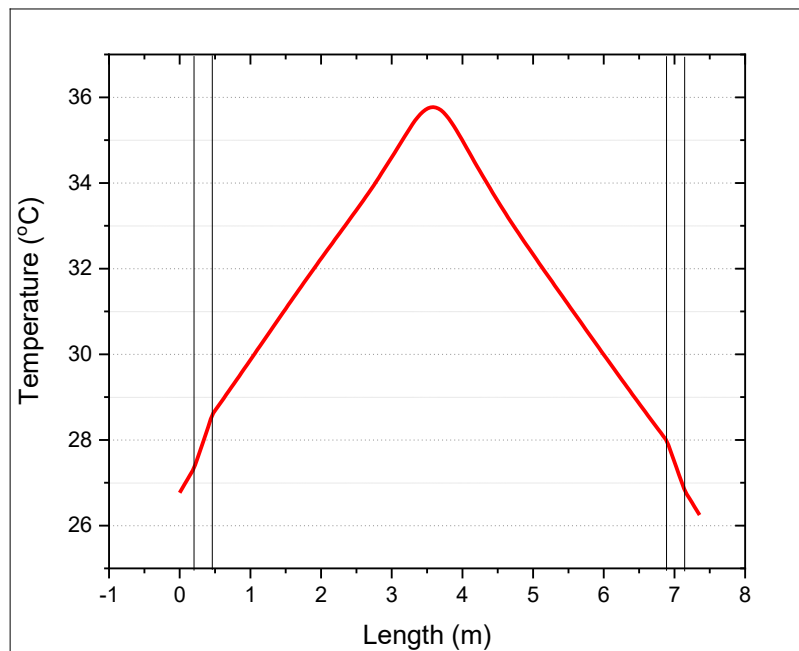


Figure 40: Temperature along central path in simplified human forearm

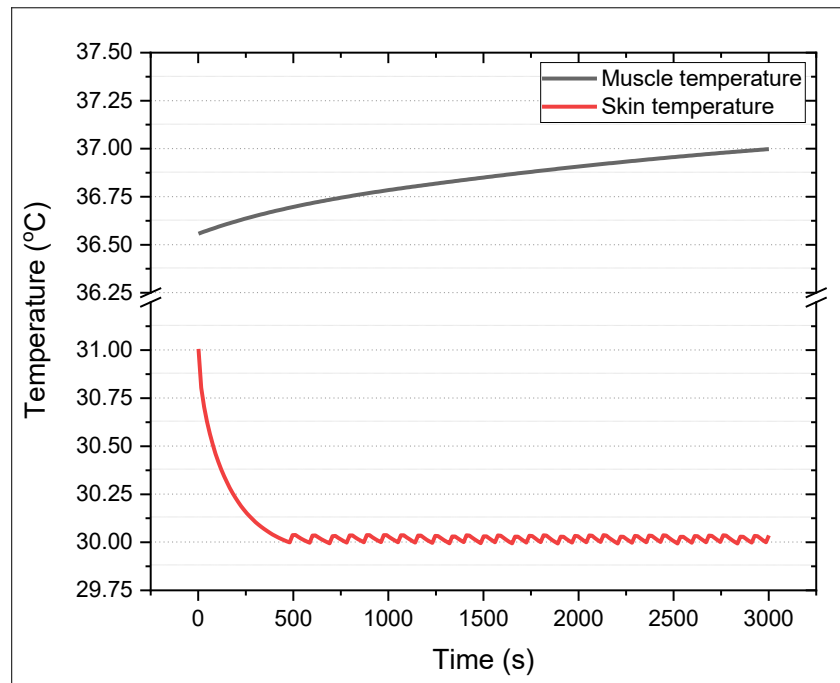


Figure 41: Muscle and skin temperature over time at 15 $^{\circ}\text{C}$

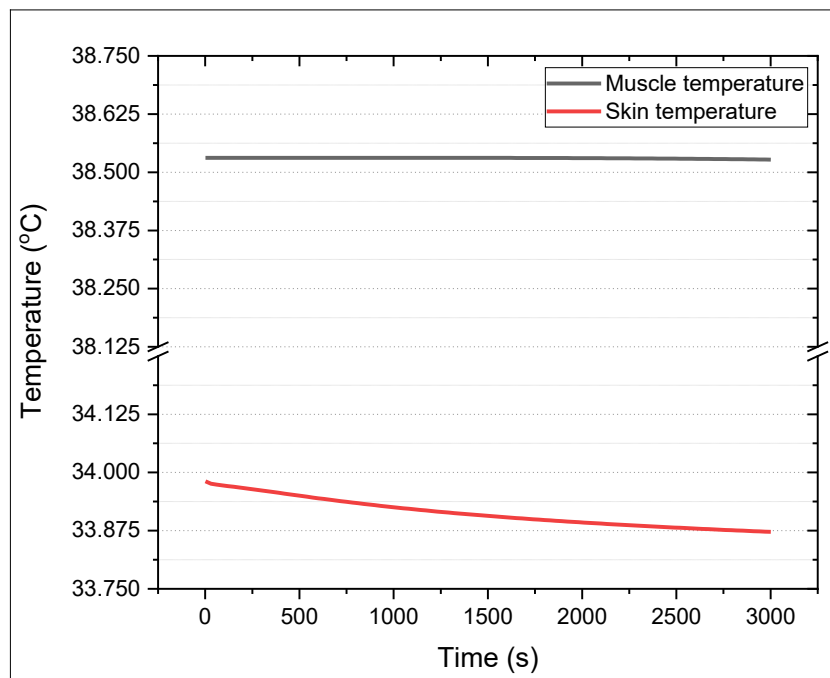


Figure 42: Muscle and skin temperature over time at 25 $^{\circ}\text{C}$